Electronic Supplementary Material (ESI) for Dalton Transactions.


# Comparisons of $MN_2S_2$ vs. Bipyridine as Redox-Active Ligands to Manganese and Rhenium in (L--L)M'$(CO)_3$Cl Complexes

Allen M. Lunsford,[a] Kristina F. Goldstein,[a] Matthew Cohan,[a] Jason A. Denny,[a]

Nattamai Bhuvanesh,[a] Shengda Ding,[a] Michael B. Hall,[a] Marcetta Y. Darensbourg*[a]

* Corresponding authors

[a] Department of Chemistry, Texas A&M University, College Station, Texas, USA

E-mail: marcetta@chem.tamu.edu

**UV-Vis Spectroscopy**



**IR Spectroscopy**



**Crystallography**

**Computational Chemistry**



**General Procedures**

All reactions and manipulations were performed using standard Schlenk-line and syringe/rubber septa techniques under $N_2$ or in an Ar atmosphere glovebox. Solvents were purified and degassed via a Bruker solvent system. Reagents were purchased from commercial sources and used as received. The $MN_2S_2$ complexes were synthesized following previously published procedures; Fe(NO)(bme-dach)[1], Co(NO)(bme-dach)[1], and Ni(bme-dach)[2]. Elemental analyses was performed by Atlantic Microlab, inc., Norcross, Georgia, United States. Electrospray ionization mass spectrometry (ESI-MS) was performed by the Laboratory for Biological Mass Spectrometry at Texas A&M University. Infrared spectra were recorded on a Bruker Tensor 37 spectrometer using a $CaF_2$ solution cell of 0.2 mm path length. UV-visible spectra were obtained using a Shimadzu UV-2450 spectrophotometer with 1.0 cm path length quartz cells. CW EPR spectrum were recorded using an X-Band Bruker 300E spectrometer. Measurement conditions: Microwave frequency: 9.3701 GHz; Modulation amplitude: 0.3 mT; Microwave power: 0.04mW. Temperature: 298 K. Spectrum were simulated using SpinCount developed by Prof. M. P. Hendrich of Carnegie Mellon University.

**Computational Methodology**

The functional B3LYP[3] was used in Gaussian 09 Revision D1[4] to execute all the calculations. Triple-ζ 6-311++G(d,p) basis set was used for all non-metal atoms[5-7] and Wachters-Hay basis set with diffuses functions and polarization functions was applied, under the designation 6-311++G(d,p) were used for transition metals Fe, Co and Ni.[8-10] The pseudopotential ECP60MDF and basis set cc-pVTZ-PP[11] were applied for Re. The crystal structures of **[Fe-Re]**, **[Co-Re]** and **[Ni-Re]** were imported as references. All the stationary points were optimized in gas phase and verified by frequency calculations with appropriate numbers of imaginary vibrations. Thermal corrections and solvation corrections (with SMD model[J], in DMF) were added to calculate Gibbs free energy. The standard reduction potential $E$ (vs. $Fc^{+/0}$) was calculated by the following equation.

$$E = -\frac{G(Red) - G(Ox) + G(Fc^+) - G(Fc)}{nF}$$

*G* is the calculated Gibbs free energy, *n* is the equivalents of electrons transferred, *F* is the Faraday constant.

**Cyclic Voltammetry**

A Bioanalytical Systems 100 electrochemical workstation with a glassy carbon working electrode (0.071 $cm^2$) and a platinum wire auxiliary electrode was used to conduct the electrochemical analysis of all compounds. A standard three electrode cell under an Ar atmosphere at room temperature was used to obtain all voltammograms. Cyclic voltammograms of all complexes as well as starting materials were recorded in 2 mM solutions with 100 mM [n-$Bu_4N$][$PF_6$] as the supporting electrolyte in the solvent indicated in the figure caption. The potentials were measured relative to a $Ag/AgNO_3$ electrode using a glassy carbon working electrode, and are referenced to $Cp_2Fe$/ $Cp_2Fe^+$ ($E_{1/2}$ = 0.00 V).

**X-ray Structure Analysis**

Low temperature (150 K) X-ray data was obtained on a Bruker Apex-II CCD based diffractometer (Texas A&M University) (Mo sealed X-ray tube, $K_\alpha$ = 0.71073 Å) for complexes A-D. Crystal samples were coated in mineral oil, affixed to a Nylon loop, and placed under streaming $N_2$. Space groups were determined on the basis of systematic absences and intensity statistics, and structures were solved by direct methods and refined by full-matrix least-squares on $F_2$. All non-hydrogen atoms were refined with anisotropic thermal parameters. H atoms were placed at idealized positions and refined with fixed isotropic displacement parameters; anisotropic displacement parameters were employed for all non-hydrogen atoms. The following programs were used: data collection, APEX2;[12] data reduction, SAINT;[13] absorption correction SADABS;[14] cell refinement SHELXTL;[14] structure solutions, SHELXS-97;[14] and structure refinement, SHELXL-97.[14] The final data presentation and structure plots were generated in X-Seed Version 2.0.[15]

**Synthesis**

Synthesis of **[Ni-Re]**: To a schlenk flask containing 0.277 g of Ni(bme-Dach) (1.0 mmol) and 0.361 g of $Re(CO)_5Cl$ (1.0 mmol) was added 50 mL of MeOH. The flask was wrapped in aluminum foil, connected to a gas bubbler, and heated at 60˚C for 12 hours. The resulting red/orange solution (containing some suspended product) was cooled and diluted with 150 mL of diethyl ether to precipitate the remaining coral colored solid. Precipitated solid was collected and dried under vacuum to afford 0.495 g of **[Ni-Re]** corresponding to an 85% yield. X-ray quality crystals were grown by slow diffusion of diethyl ether into a concentrated DMF solution of **[Ni-Re]** at 22˚C. IR (DMF, $cm^{-1}$) ν(CO) 2010, 1897, 1883. Anal. found (calcd) for $ReNiClS_2N_2O_3C_{12}H_{18}$: C, 24.97 (24.73); H, 3.09 (3.11); N, 4.97 (4.81).

Synthesis of **[Co-Re]**: To a schlenk flask containing 0.307 g of Co(NO)(bme-Dach) (1.0 mmol) and 0.361 g of $Re(CO)_5Cl$ (1.0 mmol) was added 75 mL of dichloromethane. The flask was wrapped in aluminum foil, connected to a gas bubbler, and heated at reflux for 12 hours. Solvent was removed via vacuum and the resulting brown/green solid was chromatographed on a 12 cm. x 1.5 cm. silica gel column eluting with

10% MeOH in THF. A purple band of Co(NO)(bme-Dach) eluted first followed by **[Co-Re]** as a dark green band which was collected and the solvent removed via vacuum. The resulting dark green solid weighed 0.374 g corresponding to a 61% yield. X-ray quality crystals were grown by cooling a saturated MeCN solution of **[Co-Re]** to -30˚C overnight. IR (THF, $cm^{-1}$) ν(CO) 2015, 1907, 1893. Anal. found (calcd) for $ReCoClS_2N_3O_4C_{12}H_{18}$: C, 23.71 (23.51); H, 3.18 (2.96); N, 6.62 (6.85).

Synthesis of **[Fe-Re]**: To a schlenk flask containing 0.304 g of Fe(NO)(bme-Dach) (1.0 mmol) and 0.361 g of $Re(CO)_5Cl$ (1.0 mmol) was added 75 mL of dichloromethane. The flask was wrapped in aluminum foil, connected to a gas bubbler, and heated at reflux for 12 hours. Solvent was removed via vacuum and the resulting brown/green solid was chromatographed on a 12 cm. x 1.5 cm. silica gel column eluting with 10% MeOH in THF. A green band of Fe(NO)(bme-Dach) eluted first followed by **[Fe-Re]** as a green/brown band which was collected and the solvent removed via vacuum. The resulting green/brown solid weighed 0.35 g corresponding to a 57% yield. X-ray quality crystals were grown by cooling a saturated MeCN solution of **[Fe-Re]** to -30ºC overnight. IR (THF, $cm^{-1}$) ν(CO) 2016, 1909, 1892. Anal. found (calcd) for $ReFeClS_2N_3O_4C_{12}H_{18}$: C, 23.73 (23.63); H, 3.01 (2.97); N, 6.89 (6.89).

Synthesis of **[Ni-Mn]**: To a schlenk flask containing 0.277 g of Ni(bme-Dach) (1.0 mmol) and 0.274 g of $Mn(CO)_5Br$ (1.0 mmol) was added 50 mL of MeOH. The flask was wrapped in aluminum foil, connected to a gas bubbler, and heated at 60ºC for 12 hours. The resulting orange solution (containing some suspended orange product) was cooled and diluted with 150 mL of diethyl ether to precipitate the remaining orange solid. Precipitated solid was collected and dried under vacuum to afford 0.495 g of **[Ni-Mn]** corresponding to an 89% yield. X-ray quality crystals were grown by slow diffusion of diethyl ether into a concentrated DMF solution of **[Ni-Mn]** at 22ºC. IR (DMF, $cm^{-1}$) ν(CO) 2008, 1917, 1897. Anal. found (calcd) for $MnNiBrS_2N_2O_3C_{12}H_{18}$: C, 29.76 (29.06); H, 3.74 (3.66); N, 5.84 (5.65).

Synthesis of **[Co-Mn]**: To a schlenk flask containing 0.307 g of Co(NO)(bme-Dach) (1.0 mmol) and 0.274 g of $Mn(CO)_5Br$ (1.0 mmol) was added 75 mL of dichloromethane. The flask was wrapped in aluminum foil, connected to a gas bubbler, and heated at reflux for 12 hours. Solvent was removed via vacuum and the resulting brown/green solid was chromatographed on a 12 cm. x 1.5 cm. silica gel column eluting with 10% MeOH in THF. A purple band of Co(NO)(bme-Dach) eluted first followed by **[Co-Mn]** as a dark green band which was collected and the solvent removed via vacuum. The resulting dark green solid weighed 0.408 g corresponding to a 78% yield. X-ray quality crystals were grown by cooling a saturated MeCN solution of **[Co-Mn]** to -30ºC overnight. IR (THF, $cm^{-1}$) ν(CO) 2020, 1927, 1908. Anal. found (calcd) for $MnCoBrS_2N_3O_4C_{12}H_{18}$: C, 27.92 (27.39); H, 3.25 (3.45); N, 7.62 (7.99).

Synthesis of **[Fe-Mn]**: To a schlenk flask containing 0.304 g of Fe(NO)(bme-Dach) (1.0 mmol) and 0.274 g of $Mn(CO)_5Br$ (1.0 mmol) was added 75 mL of dichloromethane. The flask was wrapped in aluminum foil, connected to a gas bubbler, and heated at reflux for 12 hours. Solvent was removed via vacuum and the resulting brown/green solid was chromatographed on a 12 cm. x 1.5 cm. silica gel column eluting with 10% MeOH in THF. A green band of Fe(NO)(bme-Dach) eluted first followed by **[Fe-Mn]** as a green/brown band which was collected and the solvent removed via vacuum. The resulting green/brown solid weighed 0.356 g corresponding to a 68% yield. X-ray quality crystals were grown by cooling a saturated MeCN solution of **[Fe-Mn]** to -30ºC overnight. IR (THF, $cm^{-1}$) ν(CO) 2019, 1930, 1912. Anal. found (calcd) for $MnFeBrS_2N_3O_4C_{12}H_{18}$: C, 27.12 (27.55); H, 3.31 (3.47); N, 7.80 (8.03).

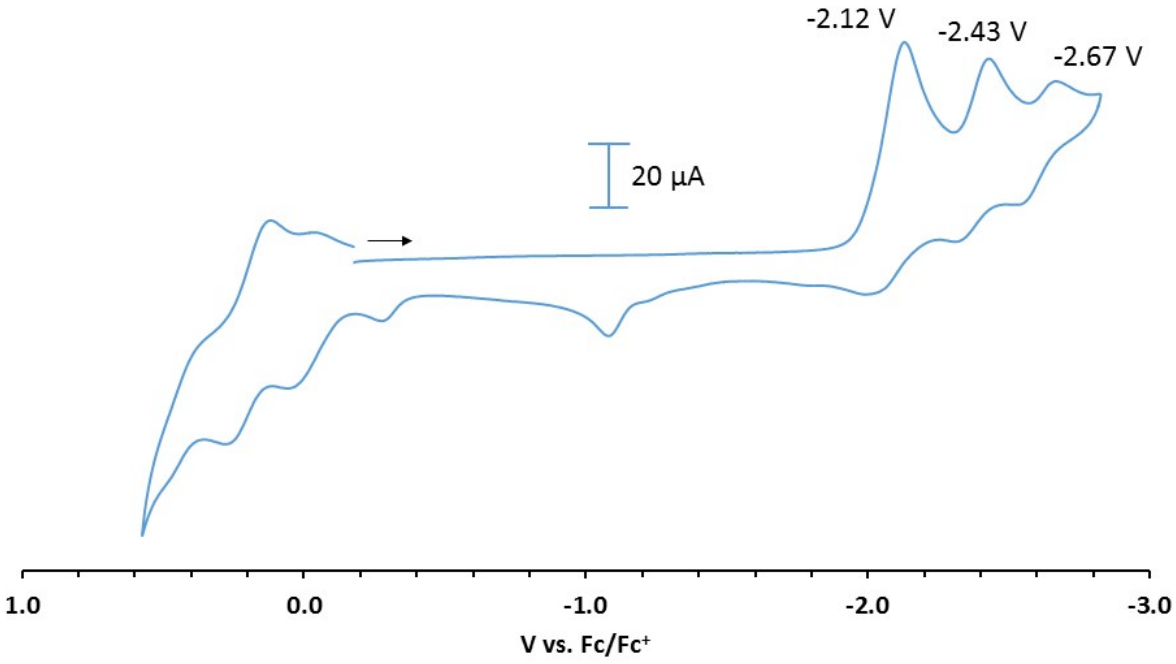


**Figure S1.** Full Scan of **[Ni-Re]** at 200 mV/s in DMF referenced to internal $Fc/Fc^+ = 0$. The scan was initiated in the negative direction.

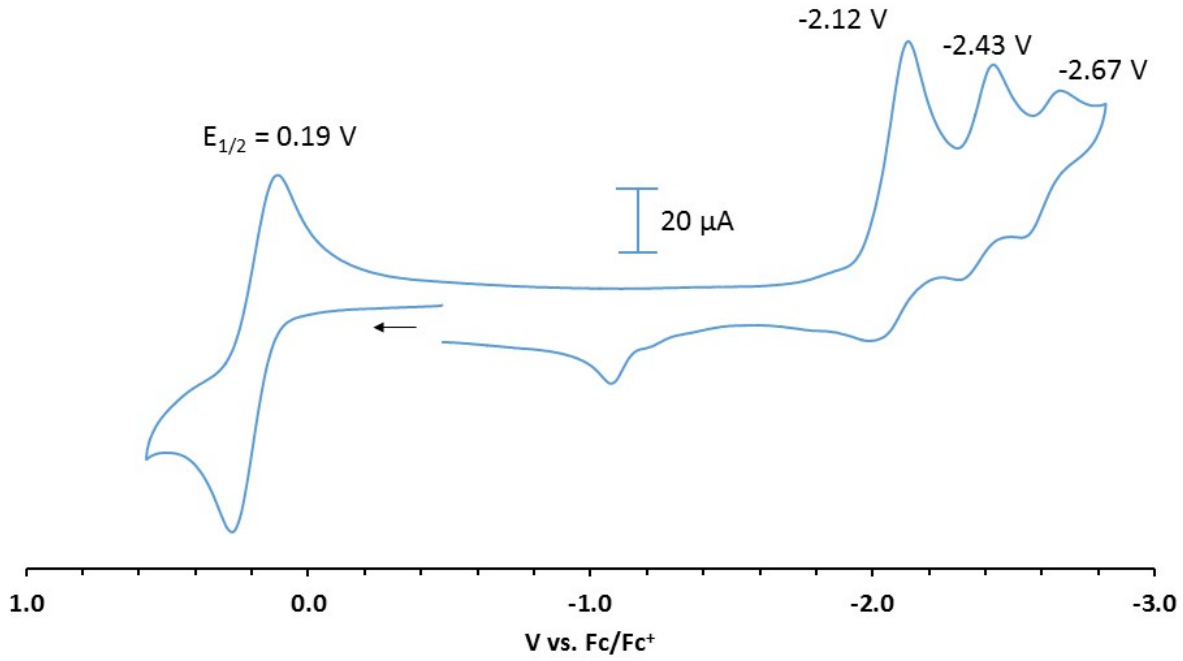


**Figure S2.** Full Scan of **[Ni-Re]** at 200 mV/s in DMF referenced to internal $Fc/Fc^+ = 0$. The scan was initiated in the positive direction.

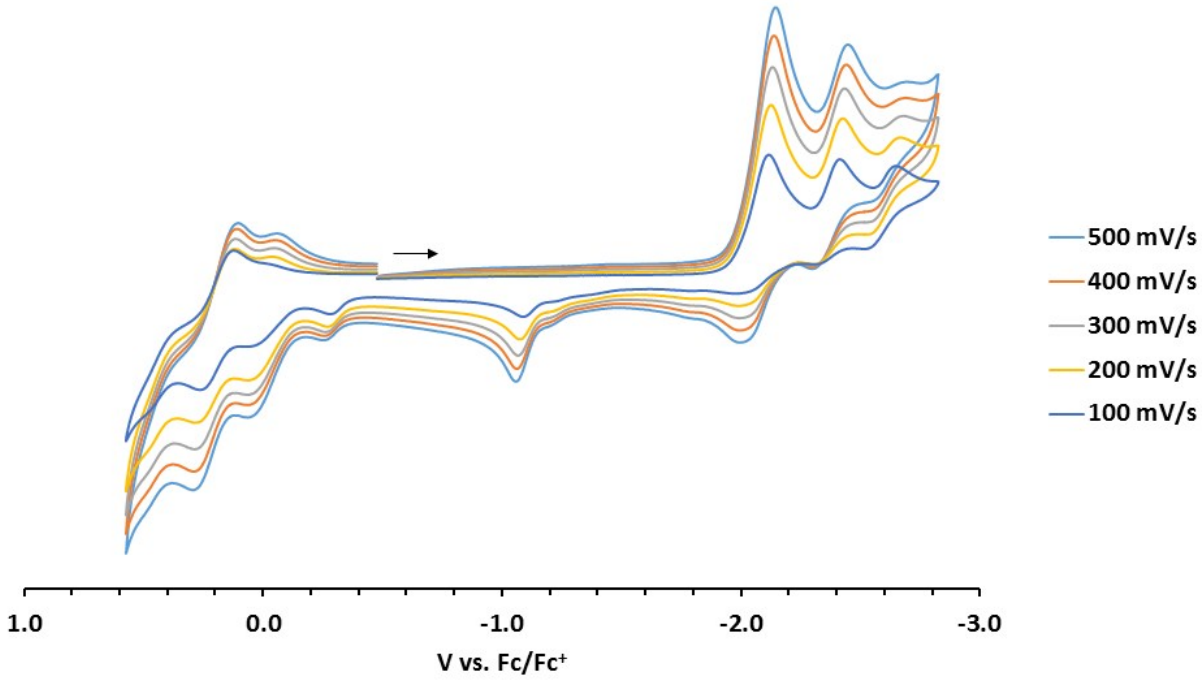


**Figure S3.** Full Scan of **[Ni-Re]** at varied scan rates in DMF referenced to internal $Fc/Fc^+ = 0$.

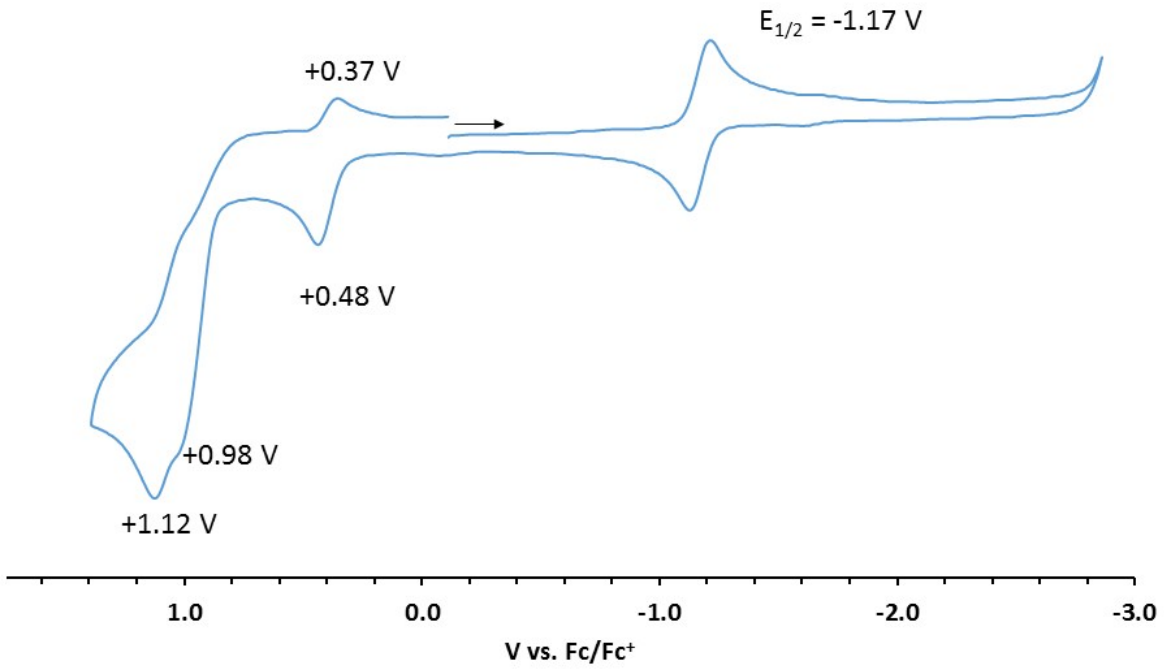


**Figure S4.** Full Scan of **[Fe-Re]** at 200 mV/s in MeCN referenced to internal $Fc/Fc^+ = 0$ initiating the scan in the negative direction.

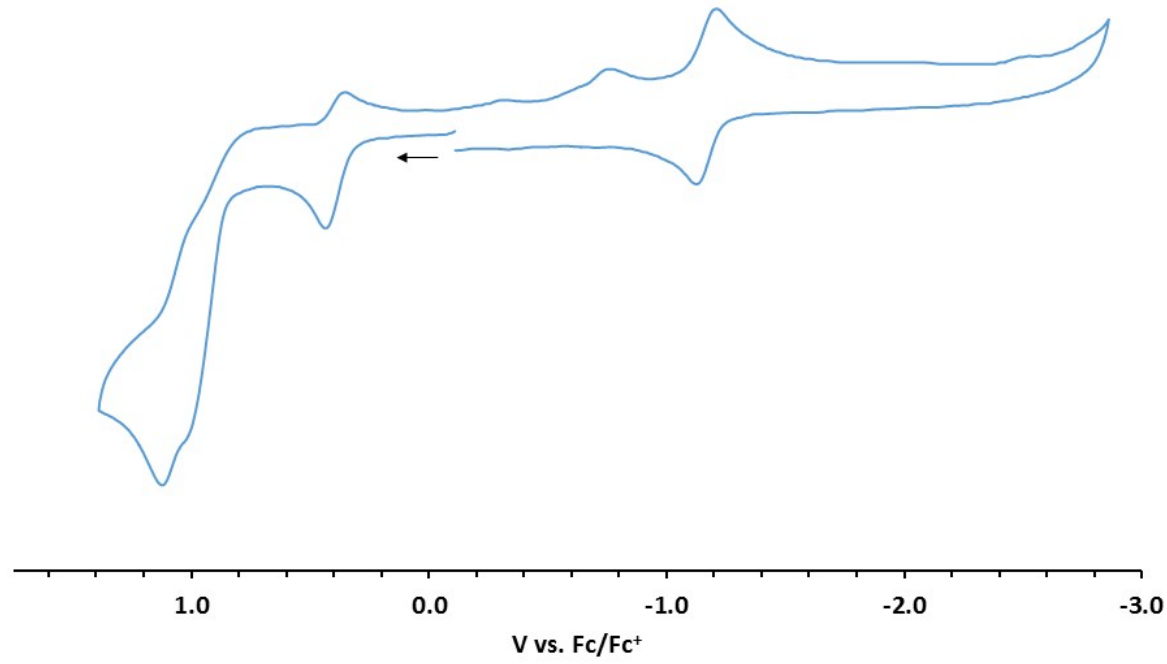


**Figure S5.** Full Scan of **[Fe-Re]** at 200 mV/s in MeCN referenced to internal $Fc/Fc^+ = 0$ initiating the scan in the positive direction.

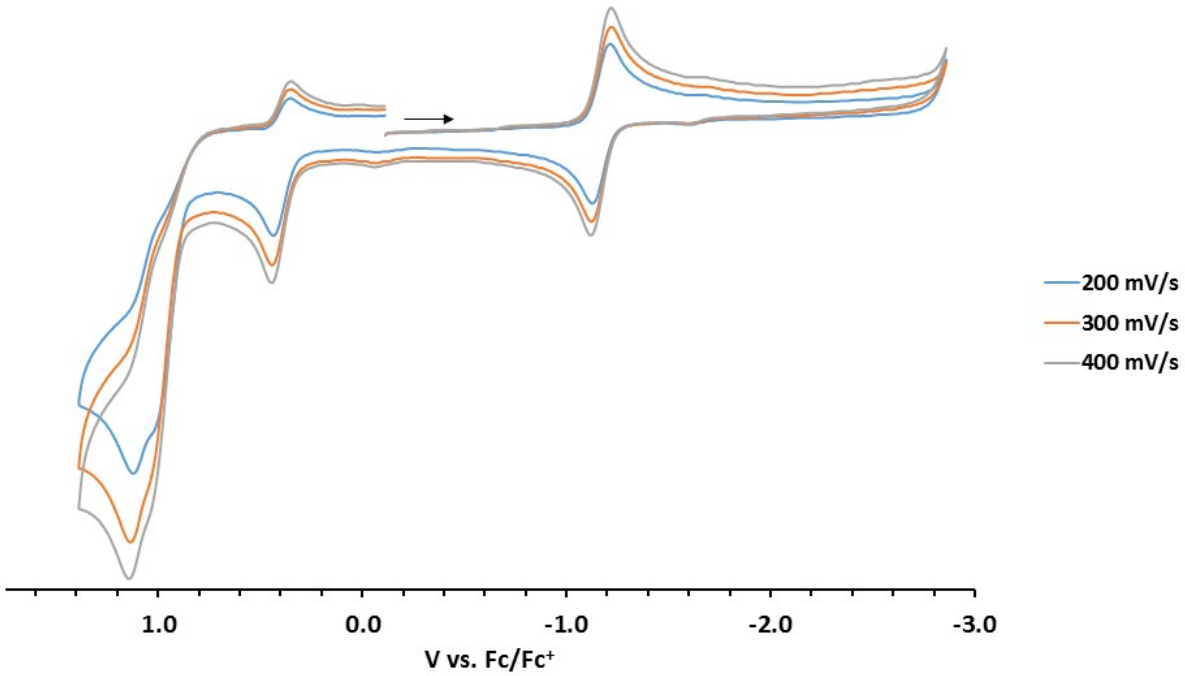


**Figure S6.** Full Scan of **[Fe-Re]** at varied scan rates in MeCN referenced to internal $Fc/Fc^{+} = 0$.

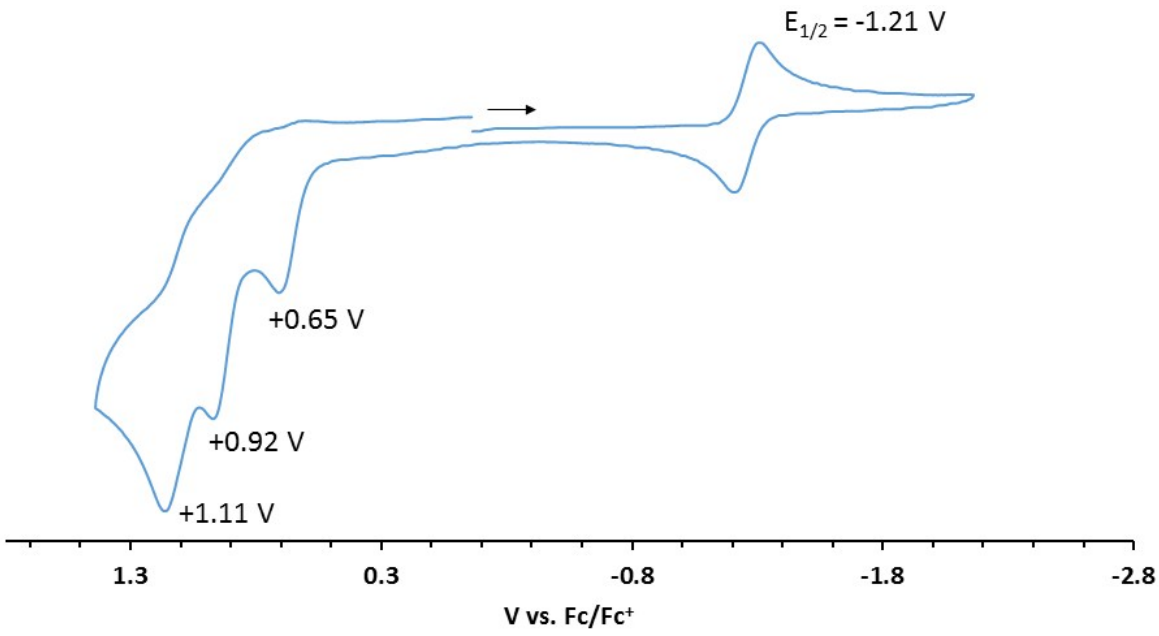


**Figure S7**. Full Scan of **[Co-Re]** at 200 mV/s in MeCN referenced to internal $Fc/Fc^{+} = 0$.

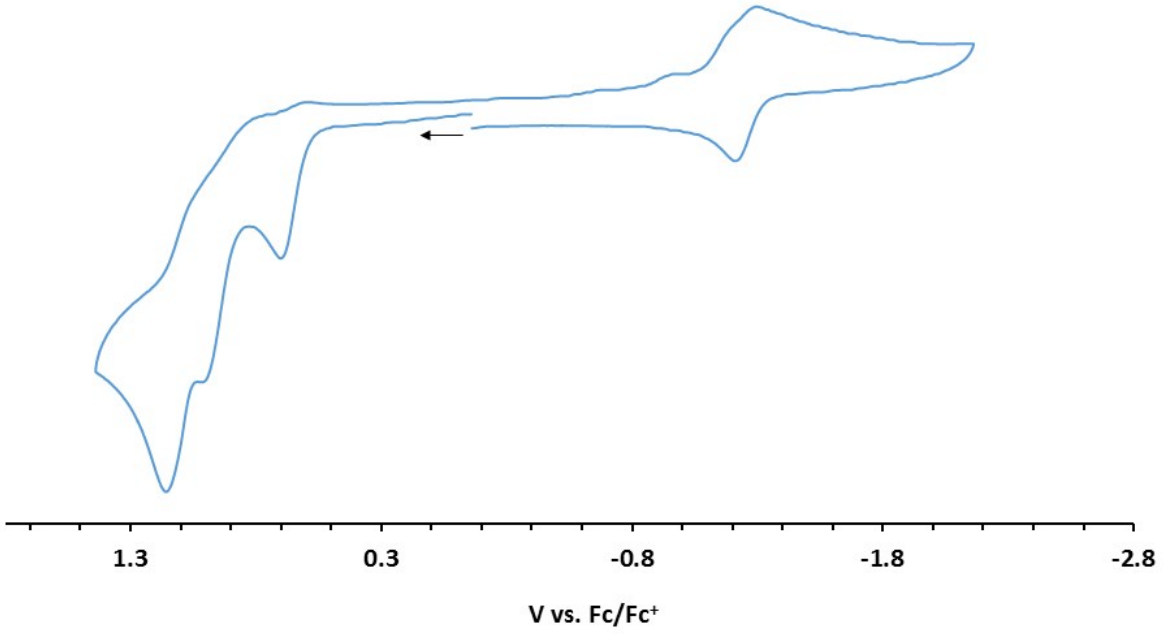


**Figure S8.** Full Scan of **[Co-Re]** at 200 mV/s in MeCN referenced to internal $Fc/Fc^+ = 0$ initiating the scan in the positive direction.

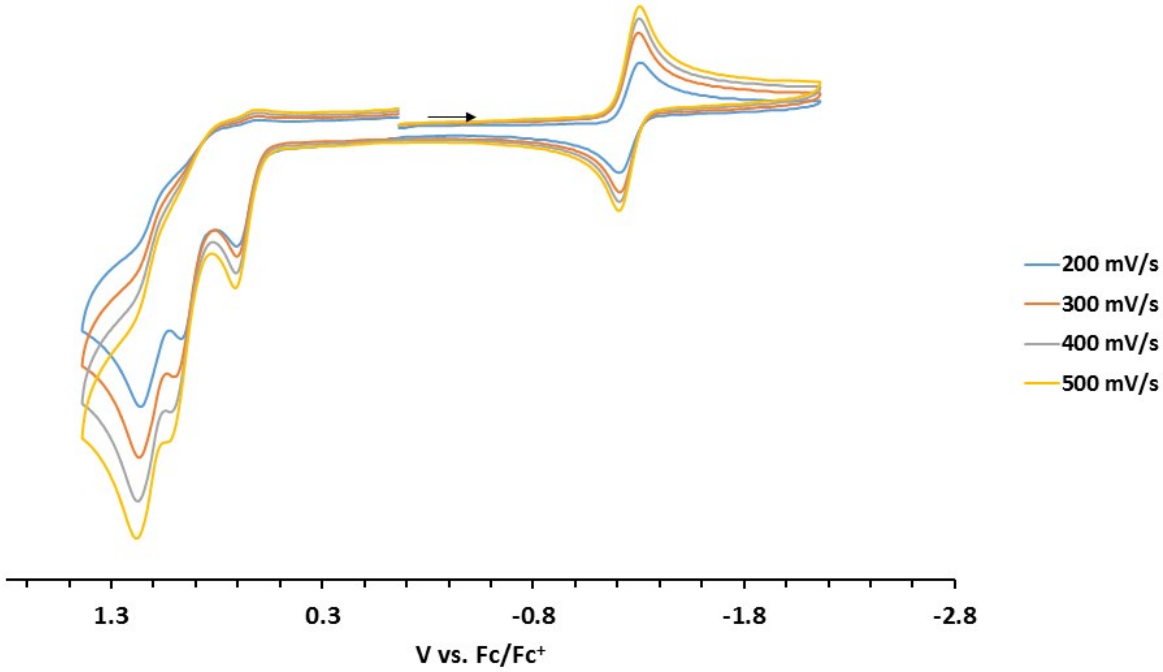


**Figure S9.** Full Scan of **[Co-Re]** at varied scan rates in MeCN referenced to internal $Fc/Fc^+ = 0$.

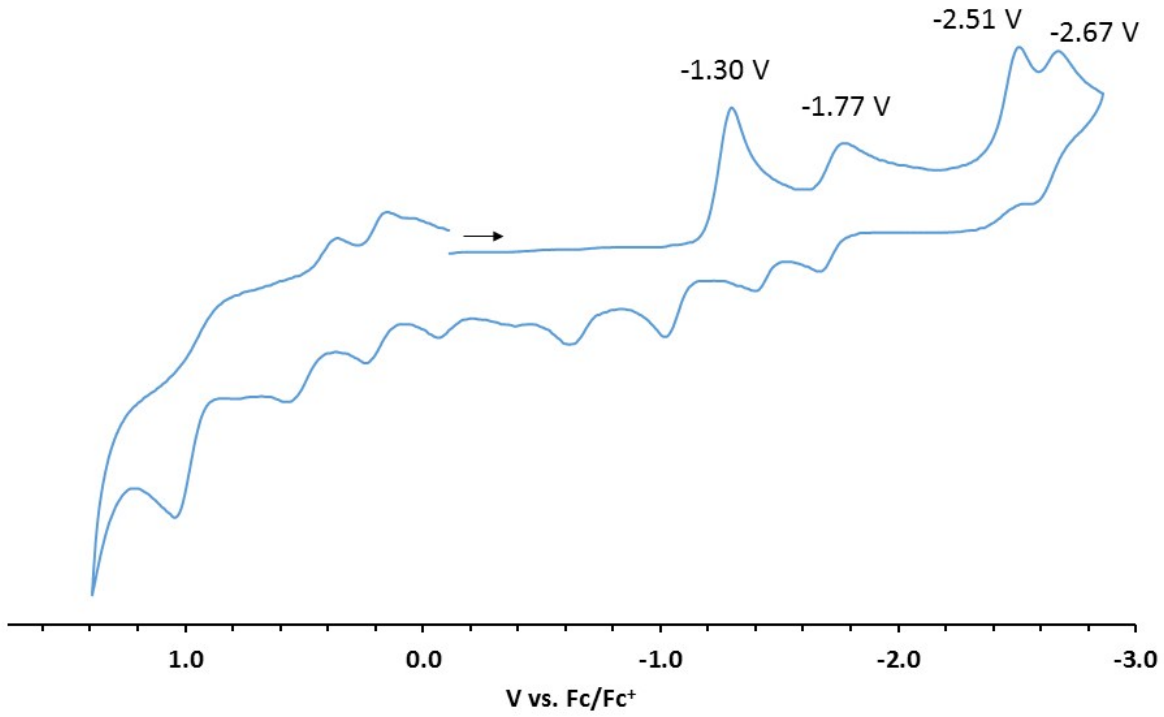


**Figure S10.** Full Scan of **[Fe-Mn]** at 200 mV/s in MeCN referenced to internal $Fc/Fc^+ = 0$ initiating the scan in the negative direction.

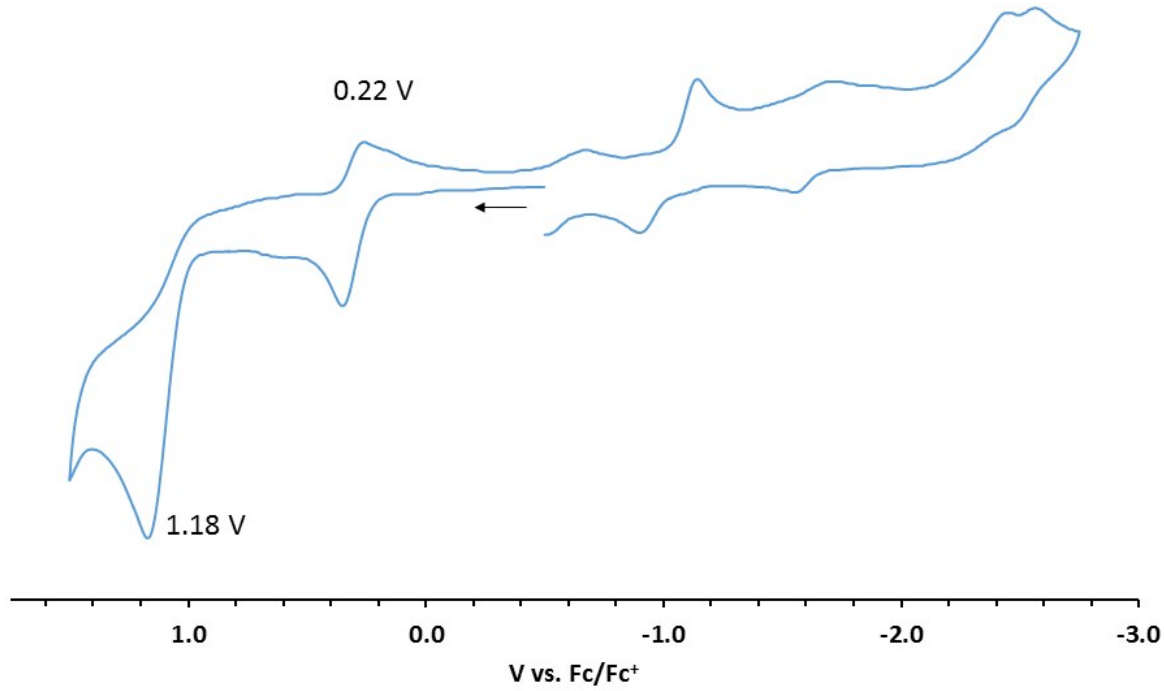


**Figure S11.** Full Scan of **[Fe-Mn]** at 200 mV/s in MeCN referenced to internal $Fc/Fc^+ = 0$ initiating the scan in the positive direction.

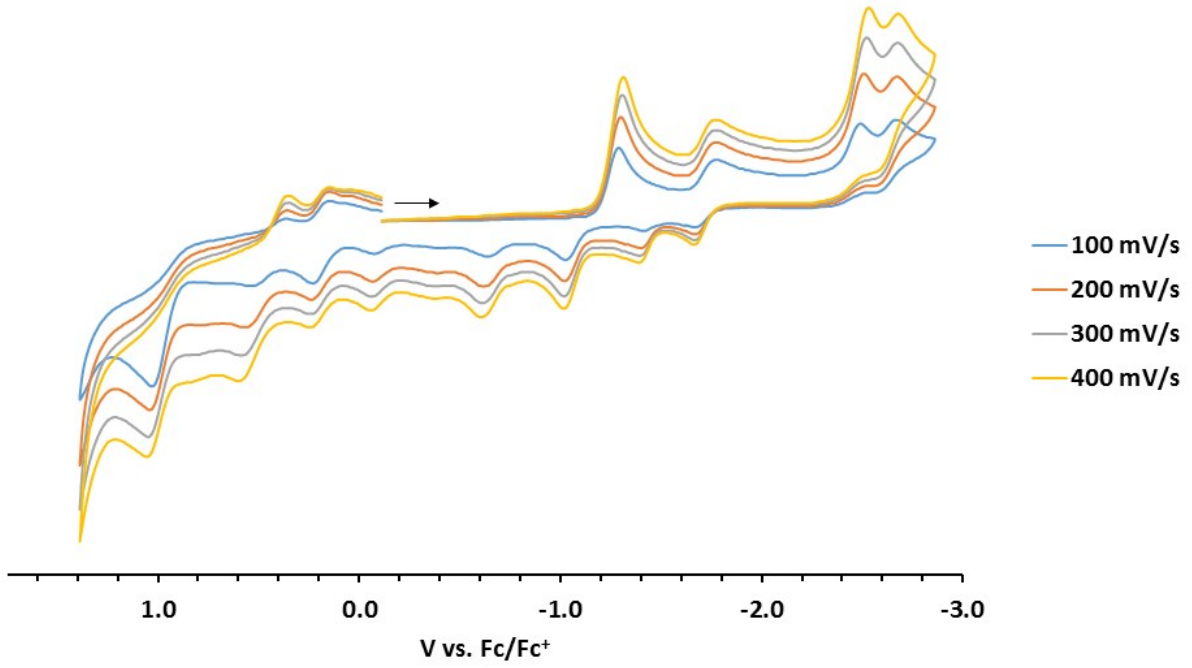


**Figure S12.** Full Scan of **[Fe-Mn]** at varied scan rates in MeCN referenced to internal $Fc/Fc^{+} = 0$.

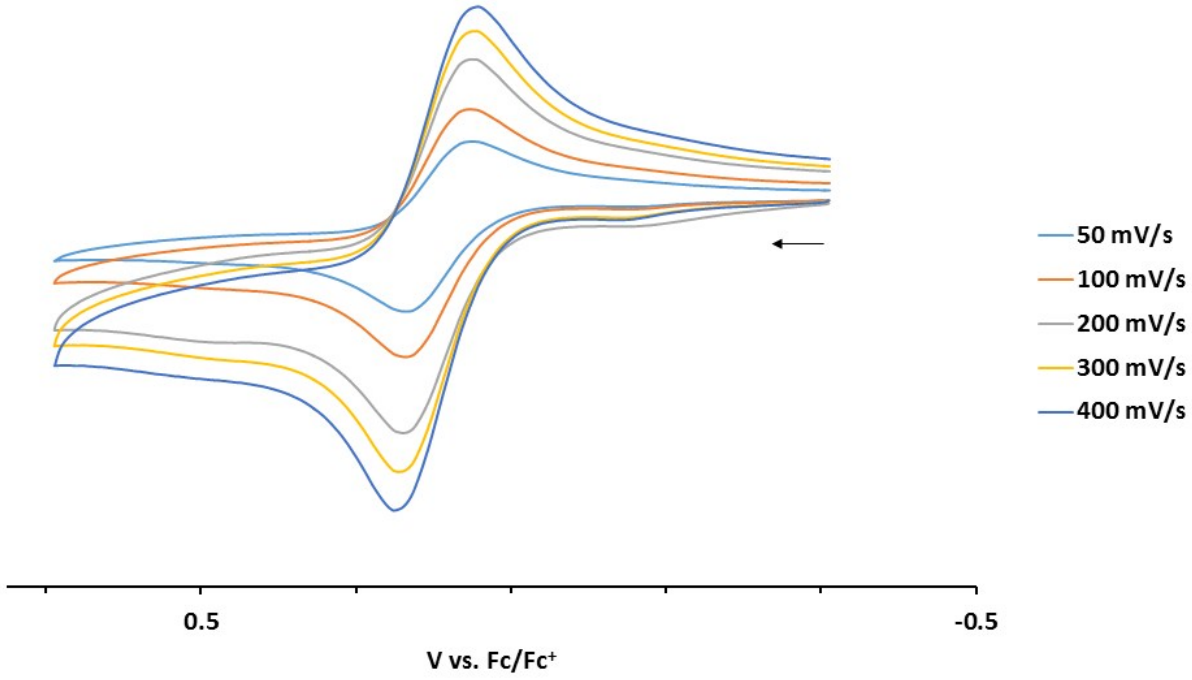


**Figure S13.** Isolated scan of **[Fe-Mn]** at varied scan rates in MeCN referenced to internal $Fc/Fc^{+} = 0$.

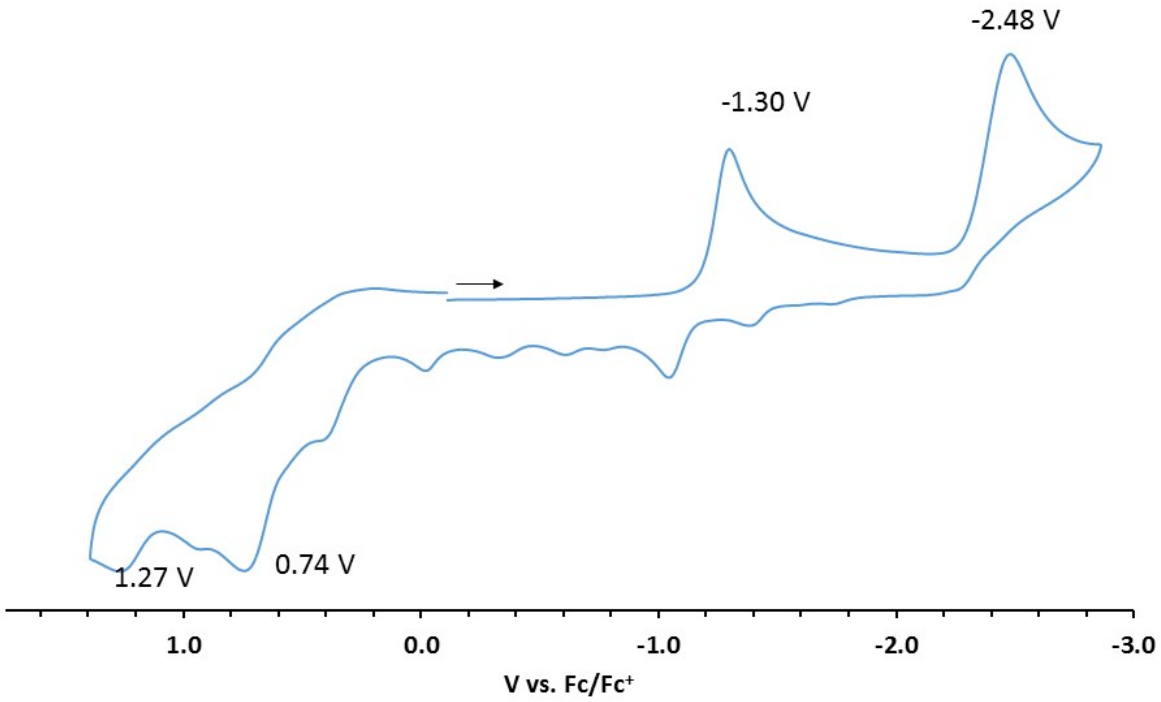


**Figure S14.** Full Scan of **[Co-Mn]** at 200 mV/s in MeCN referenced to internal $Fc/Fc^{+} = 0$ initiating the scan in the negative direction.

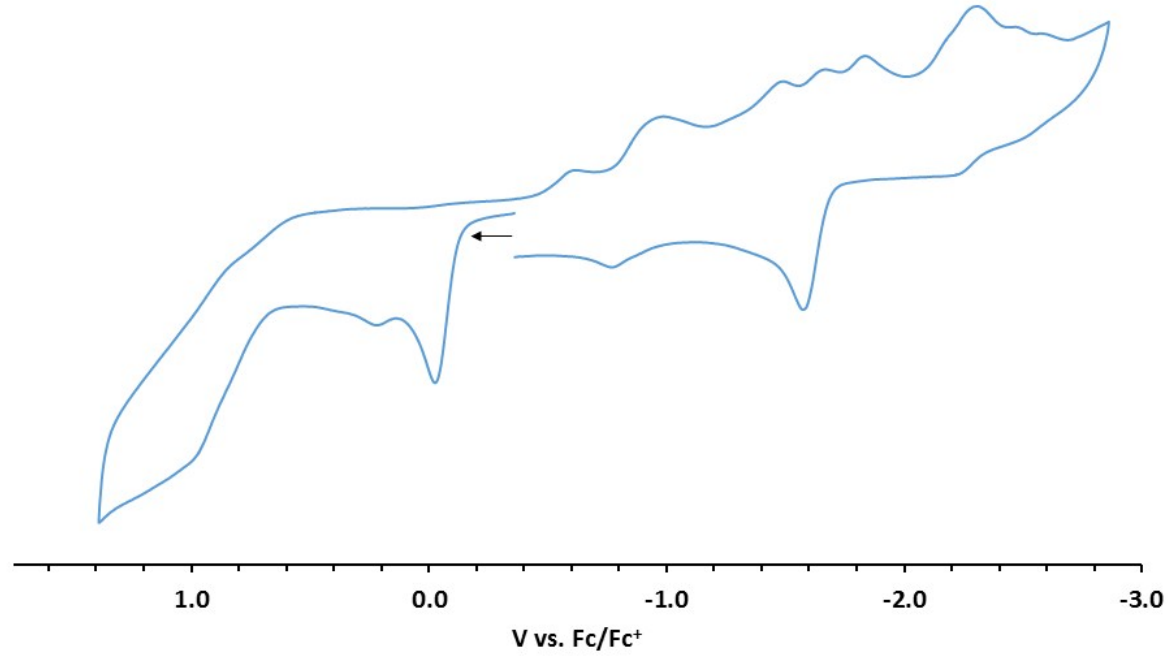


**Figure S15.** Full Scan of **[Co-Mn]** at 200 mV/s in MeCN referenced to internal $Fc/Fc^{+} = 0$ initiating the scan in the positive direction.

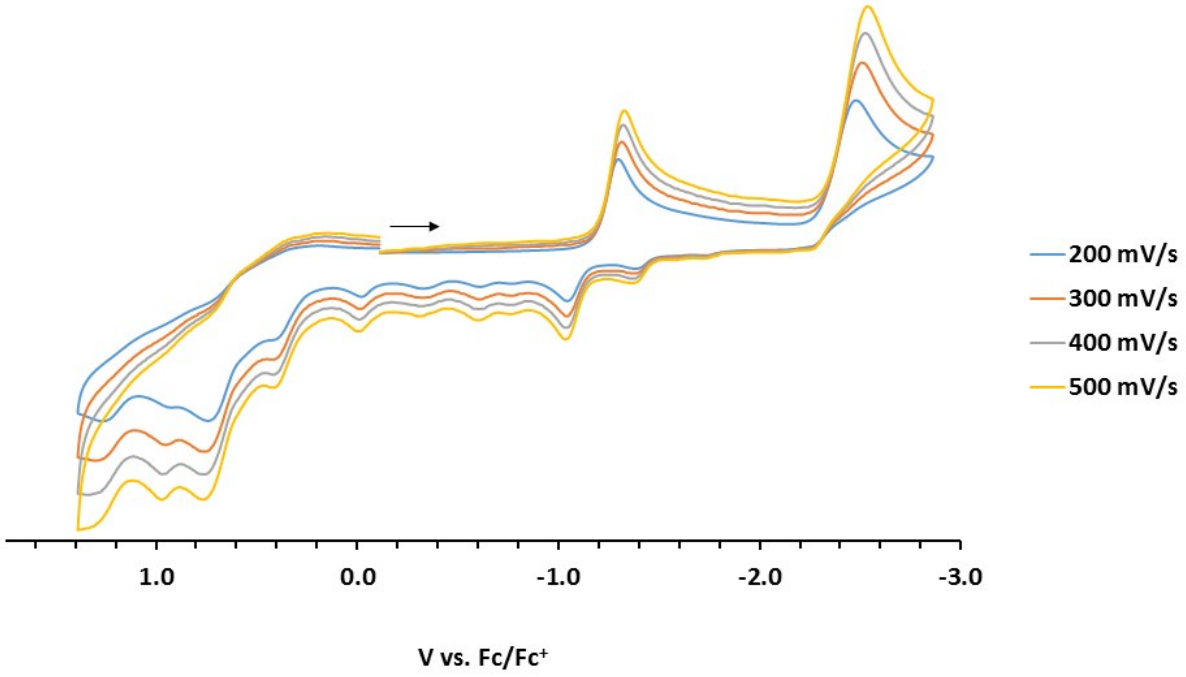


**Figure S16.** Full Scan of **[Co-Mn]** at varied scan rates in MeCN referenced to internal $Fc/Fc^{+} = 0$.

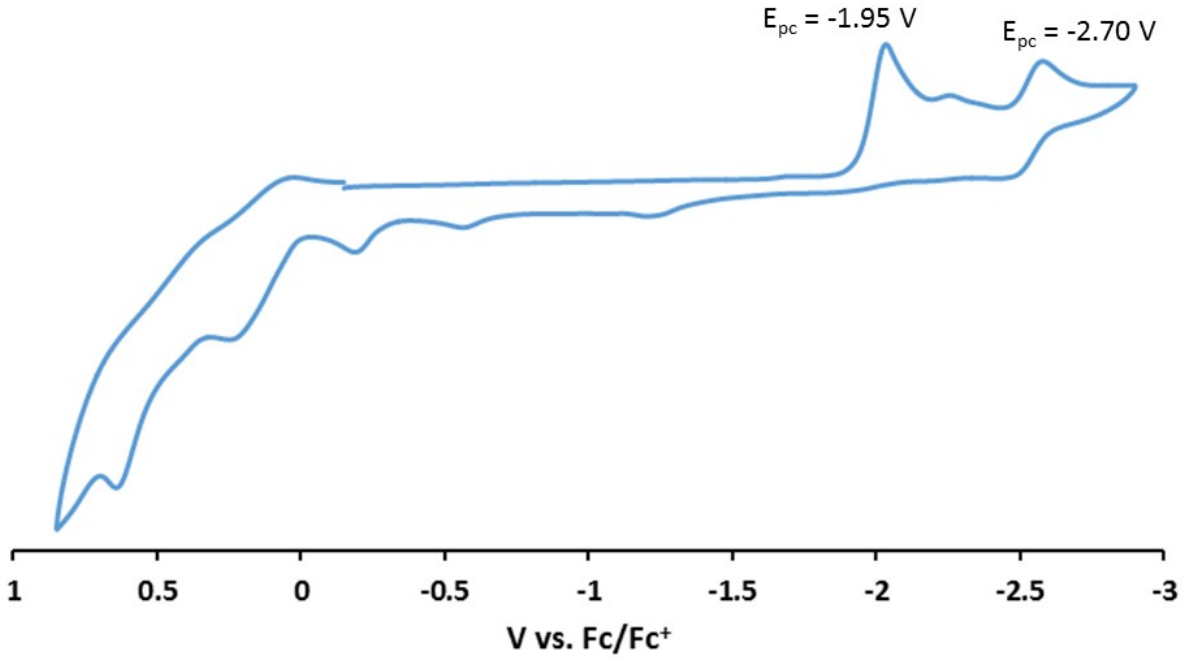


**Figure S17.** Full Scan of **[Ni-Mn]** at 200 mV/s in DMF referenced to internal $Fc/Fc^{+} = 0$ initiating the scan in the negative direction.

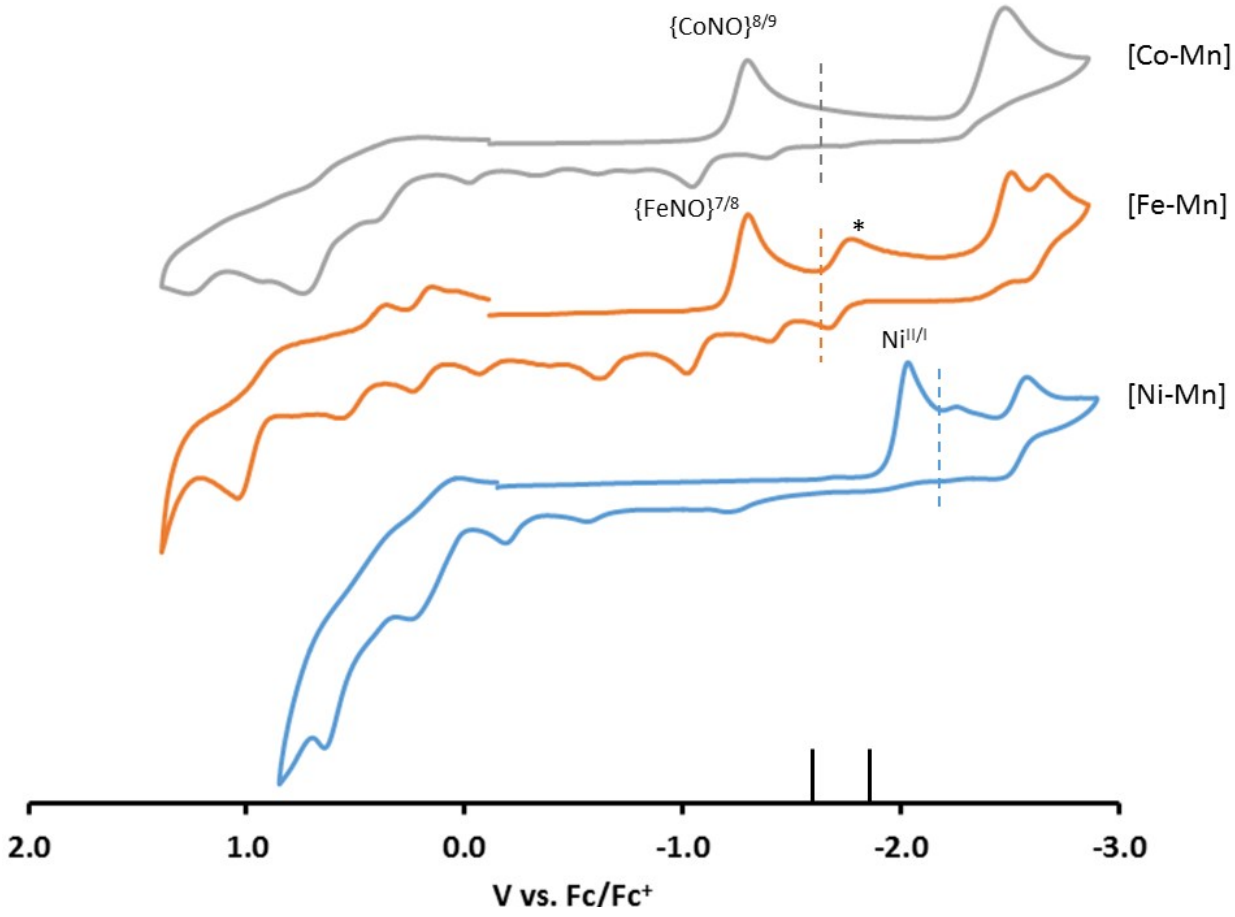


**Figure S18.** Stacked plots of the three Mn containing heterobimetallics. The dotted lines denote the reduction potential of the free $MN_2S_2$ metalloligand and the solid black lines denote the reduction potentials of $Mn(bipy)(CO)_3Br$.

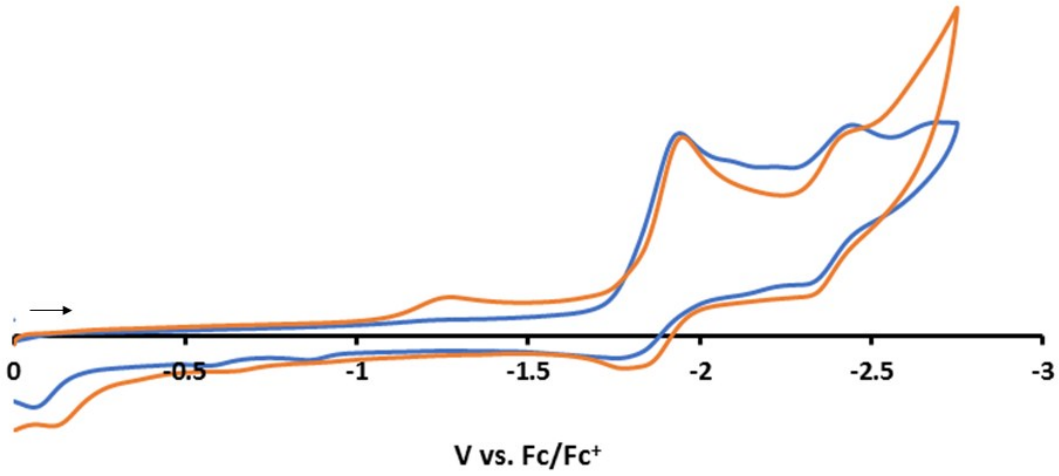


**Figure S19.** Full scan of **[Ni-Re]** at 200 mV/s in DMF with 200 equivalents of LiCl referenced to internal $Fc/Fc^+ = 0$ initiating the scan in the negative direction. The blue trace is in the absence of LiCl and the orange trace is in the presence of LiCl.

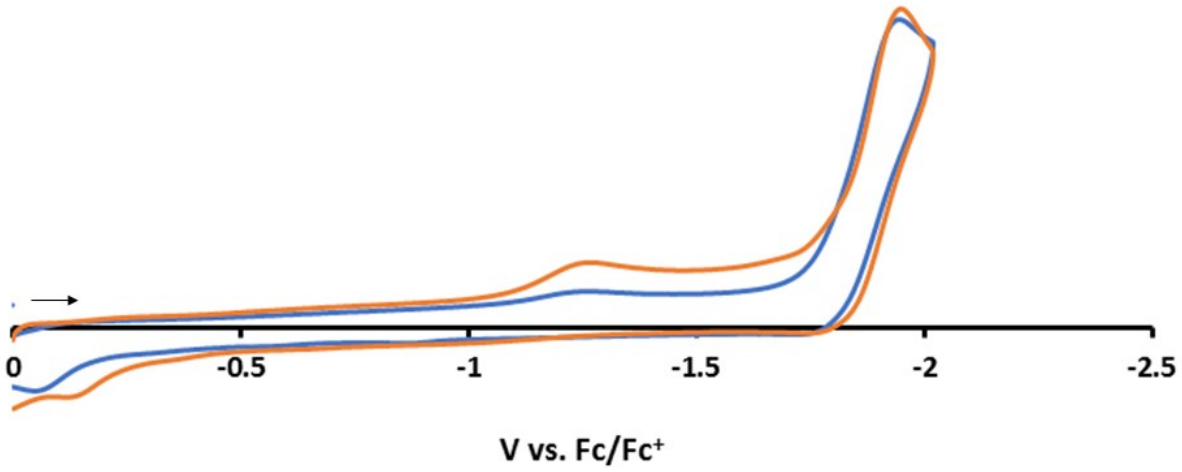


**Figure S20**. Isolated scan of **[Ni-Re]** at 200 mV/s in DMF with 200 equivalents of LiCl referenced to internal $Fc/Fc^+ = 0$ initiating the scan in the negative direction. The blue trace is in the absence of LiCl and the orange trace is in the presence of LiCl.

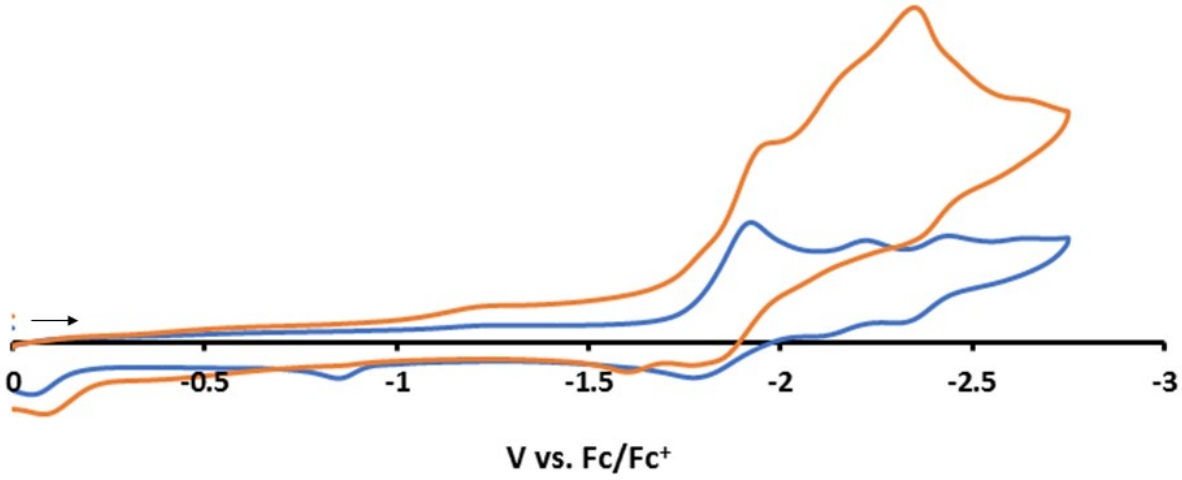


**Figure S21.** Full scan of **[Ni-Re]** at 200 mV/s in DMF with 200 equivalents of $Et_4NCl$ referenced to internal $Fc/Fc^+ = 0$ initiating the scan in the negative direction. The blue trace is in the absence of $Et_4NCl$ and the orange trace is in the presence of $Et_4NCl$.

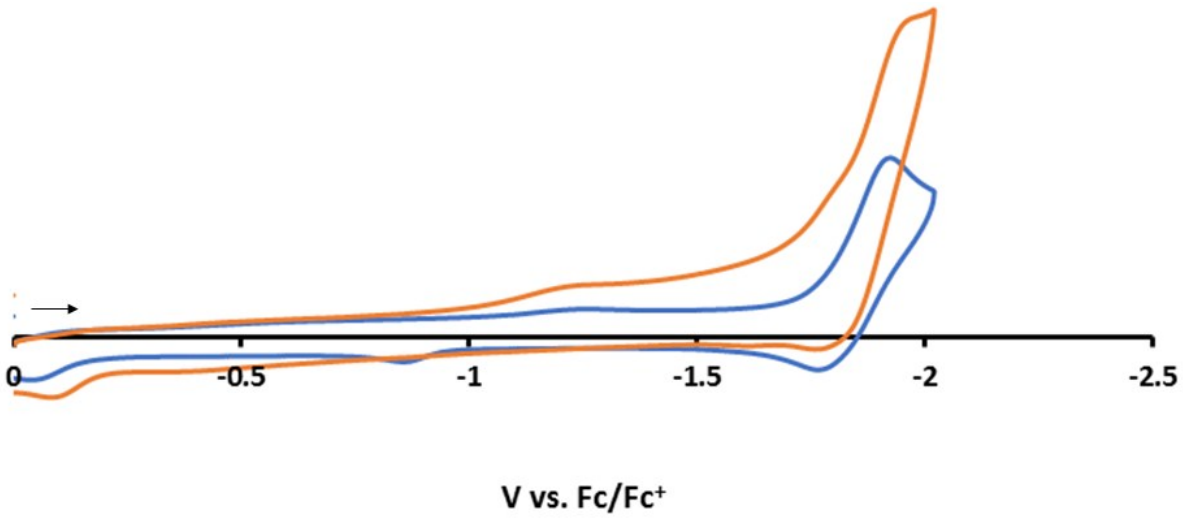


**Figure S22.** Isolated scan of **[Ni-Re]** at 200 mV/s in DMF with 200 equivalents of $Et_4NCl$ referenced to internal $Fc/Fc^+ = 0$ initiating the scan in the negative direction. The blue trace is in the absence of $Et_4NCl$ and the orange trace is in the presence of $Et_4NCl$.

**Table S1.** Reduction potentials of the six new heterobimetallic complexes, the $MN_2S_2$ starting materials, and M'(bipy)$(CO)_3X$. Also represented is the shift in the $MN_2S_2$ reduction potential upon binding the second metal center, and the shift in the Mn/Re based reduction events.

| | Reduction Events | $\Delta E_{MN2S2}$ | $\Delta E_{Re/Mn}$ |
|---|---|---|---|
| **[Ni-Re]** | -2.12 V, -2.43 V, -2.67 V | 0.22 V | 0.65 V |
| **[Fe-Re]** | -1.17 V | 0.46 V | >1.08 V |
| **[Co-Re]** | -1.21 V | 0.41 V | >1.08 V |
| Re(bipy)$(CO)_3Cl$ | -1.78 V, -2.12 V | - | - |
| **[Ni-Mn]** | -1.95 V, -2.7 V | 0.39 V | 1.03 V |
| **[Fe-Mn]** | -1.30 V, -1.77 V, -2.51 V, -2.67 V | 0.33 V | 0.84 V |
| **[Co-Mn]** | -1.30 V, -2.48 V | 0.32 V | 0.81 V |
| Mn(bipy)$(CO)_3Br$ | -1.67 V, -1.87 V | - | - |
| FeNO(bme-dach) | -1.63 V | - | - |
| CoNO(bme-dach) | -1.62 V | - | - |
| Ni(bme-Dach) | -2.34 V | - | - |

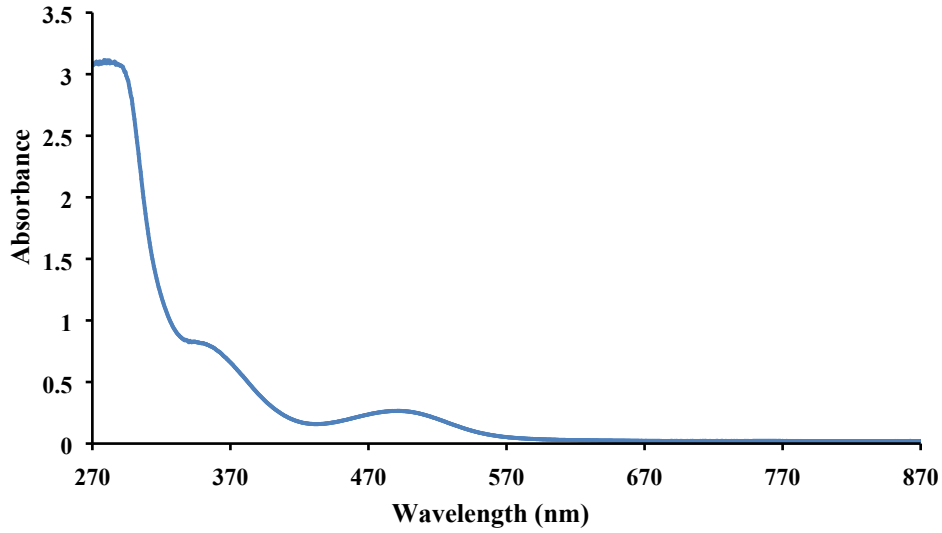


**Figure S23.** UV-Vis spectrum of **[Ni-Re]** in DMF at a concentration of 0.5 mM.

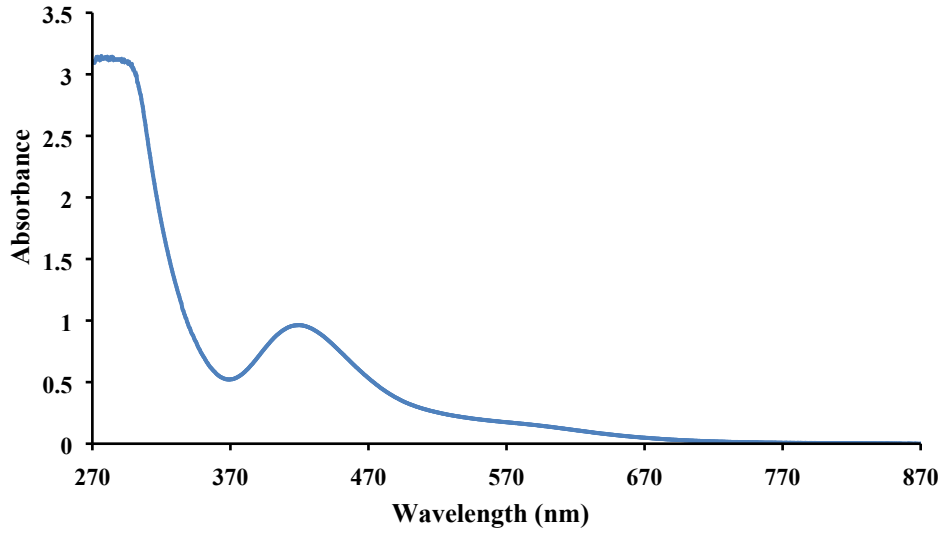


**Figure S24.** UV-Vis spectrum of **[Co-Re]** in DMF at a concentration of 0.5 mM.

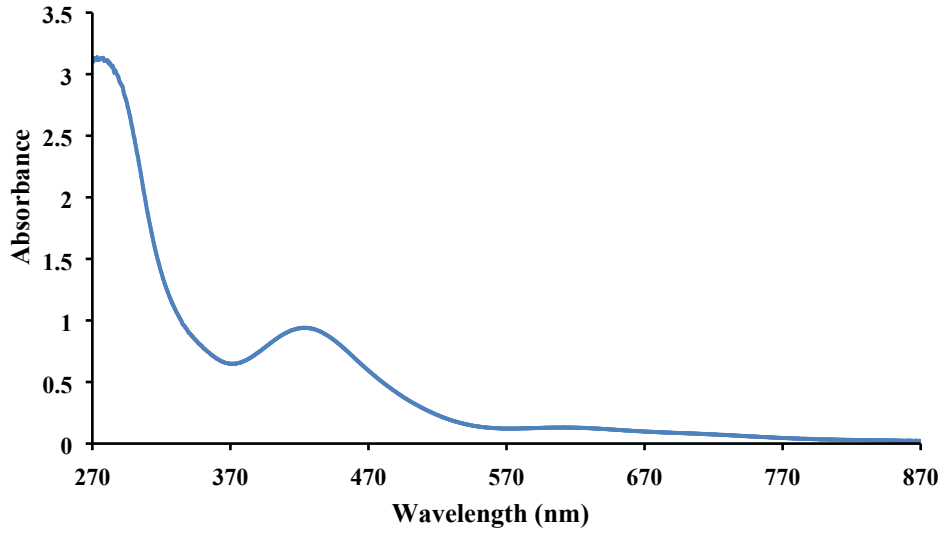


**Figure S25.** UV-Vis spectrum of **[Fe-Re]** in DMF at a concentration of 0.5 mM.

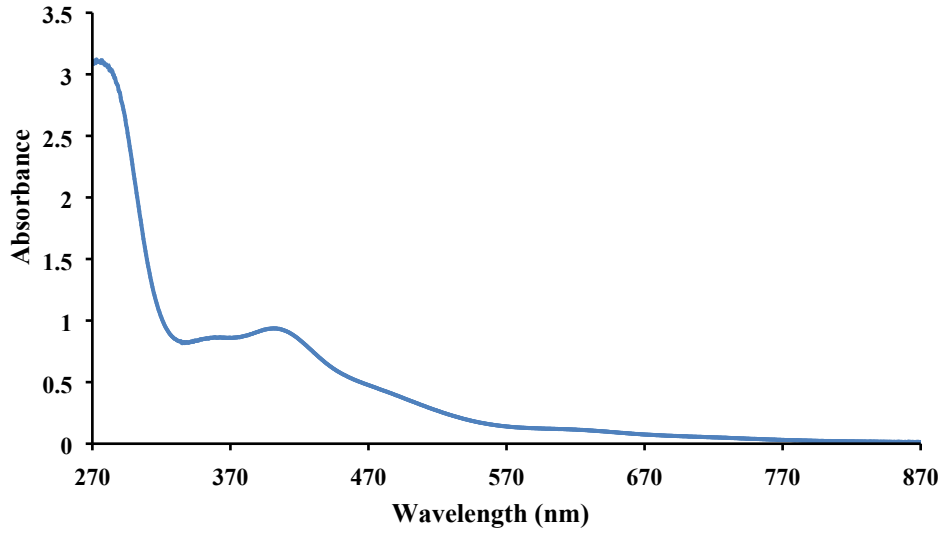


**Figure S26.** UV-Vis spectrum of **[Fe-Mn]** in DMF at a concentration of 0.5 mM.

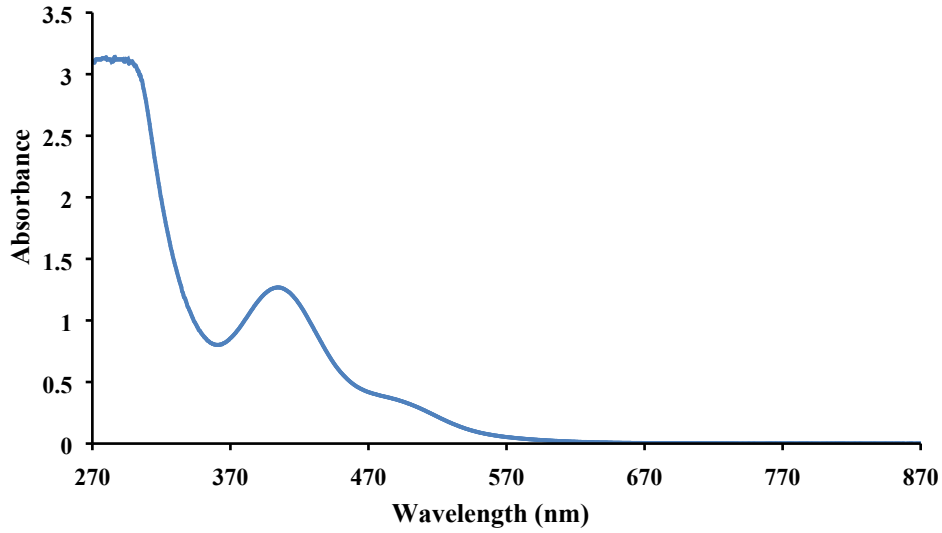


**Figure S27.** UV-Vis spectrum of **[Ni-Mn]** in DMF at a concentration of 0.5 mM.

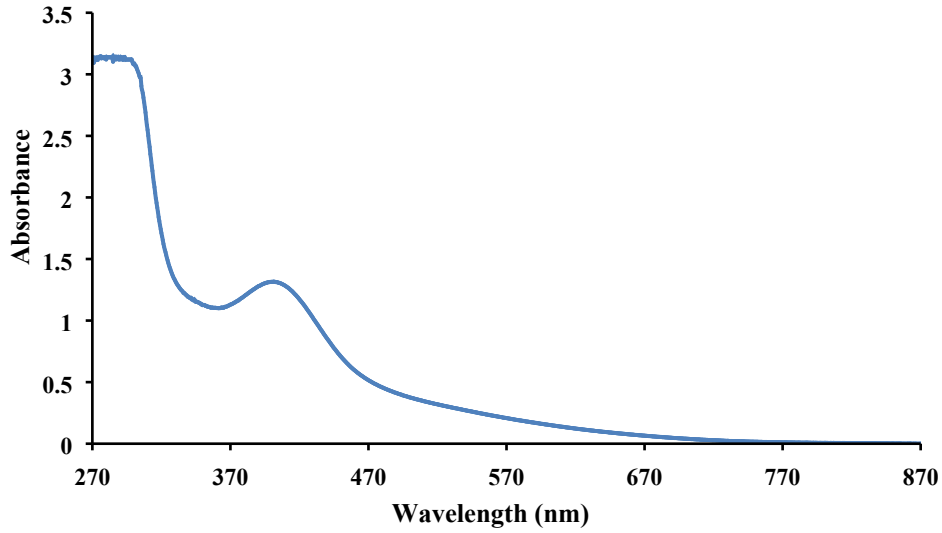


**Figure S28.** UV-Vis spectrum of **[Co-Mn]** in DMF at a concentration of 0.5 mM.

**Table S2.** Absorbances of the heterobimetallic complexes obtained from the UV-Vis spectra.

| | Wavelength (nm) |
|---|---|
| **[Ni-Re]** | 353, 491 |
| **[Fe-Re]** | 425, 610 |
| **[Co-Re]** | 420, 591 |
| **[Ni-Mn]** | 406, 495 |
| **[Fe-Mn]** | 357, 402, 620 |
| **[Co-Mn]** | 401, 546 |
| Ni(bmeDach) | 457 |
| $Mn(bipy)(CO)_3Br$ | 415 |
| $Re(bipy)(CO)_3Cl$ | 330 |

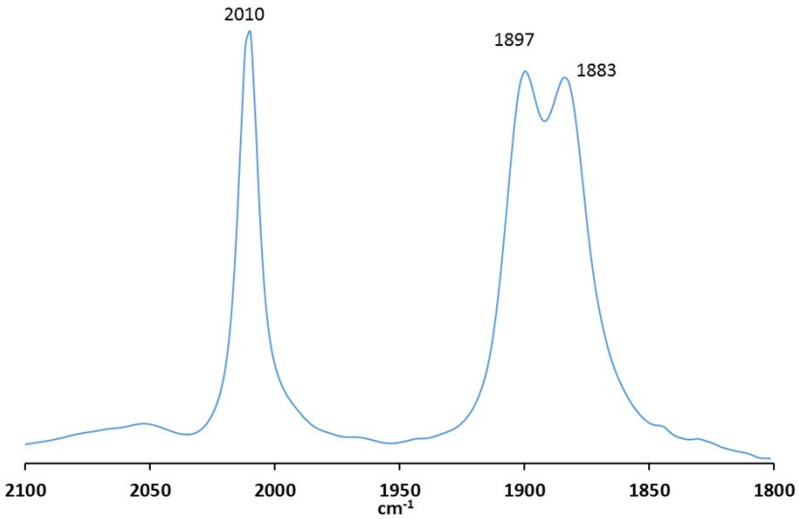


**Figure S29.** IR Spectrum of **[Ni-Re]** in DMF.

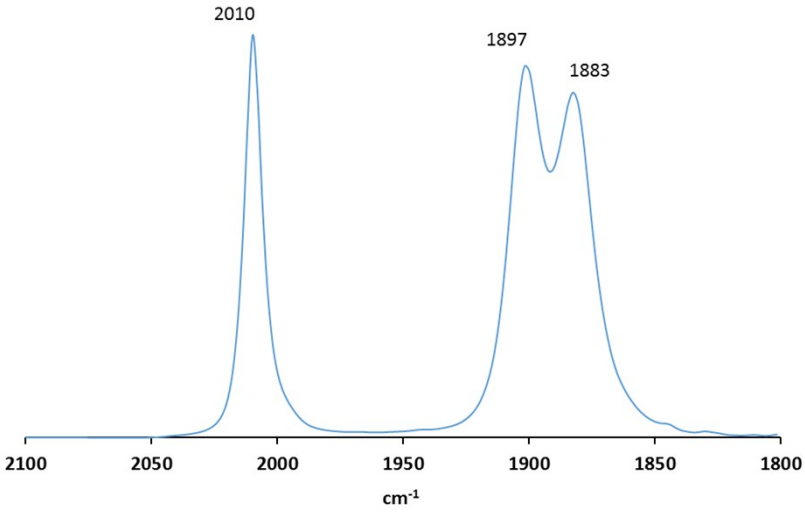


**Figure S30.** IR Spectrum of NiDacoRe in DMF.

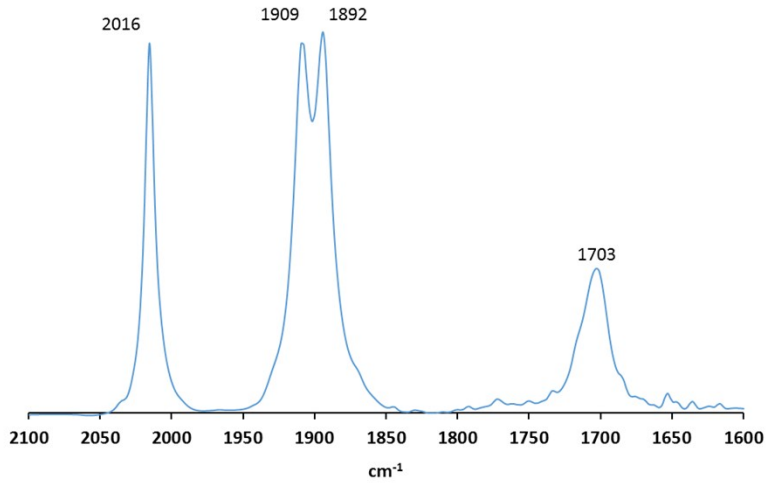


**Figure S31.** IR Spectrum of **[Fe-Re]** in THF.

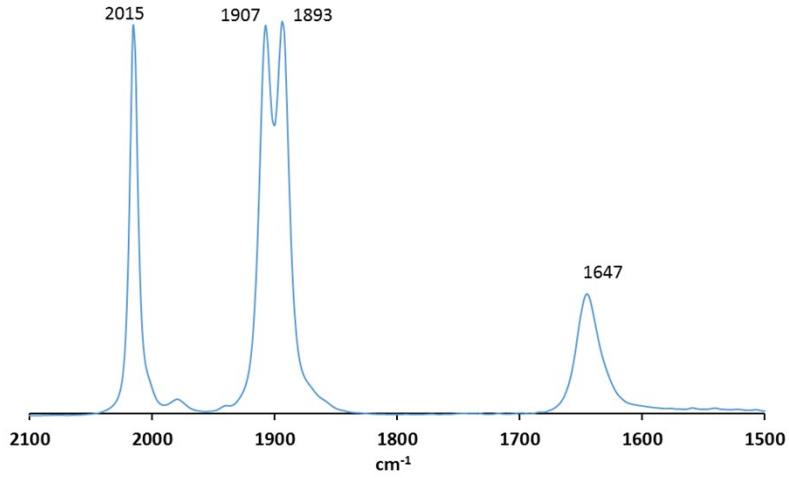


**Figure S32.** IR Spectrum of **[Co-Re]** in THF.

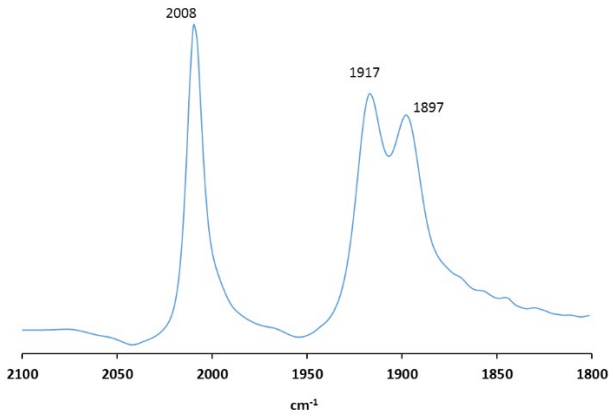


**Figure S33.** IR Spectrum of **[Ni-Mn]** in DMF.

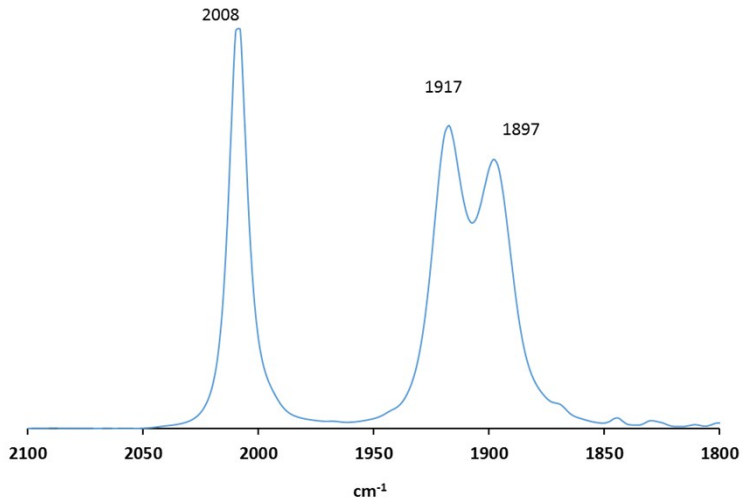


**Figure S34.** IR Spectrum of NiDacoMn in DMF.

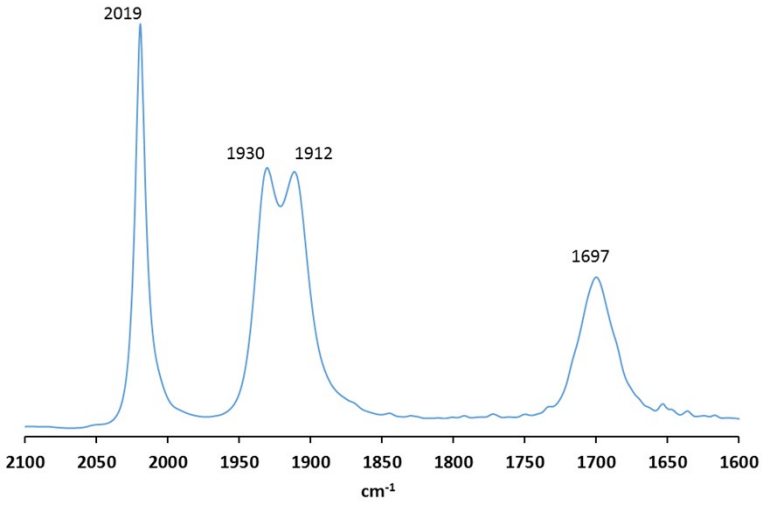


**Figure S35.** IR Spectrum of **[Fe-Mn]** in THF.

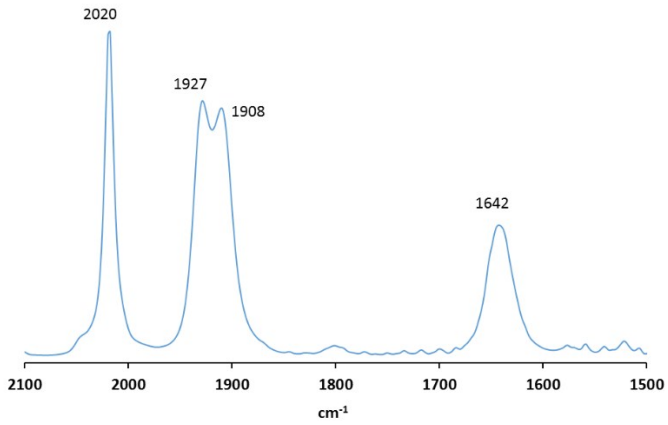


**Figure S36.** IR Spectrum of **[Co-Mn]** in THF.

**Table S3.** List of ν(CO) and ν(NO) stretching frequencies of the heterobimetallic complexes, the $MN_2S_2$ starting materials and the analogous bipy complexes.

| | CO ($cm^{-1}$) | NO ($cm^{-1}$) |
|---|---|---|
| **[Ni-Re]** | 2010, 1897, 1883 | |
| **[Fe-Re]** | 2016, 1909, 1892 | 1703 |
| **[Co-Re]** | 2015, 1907, 1893 | 1647 |
| $Re(bipy)(CO)_3Cl$ | 2019, 1914, 1893 | |
| **[Ni-Mn]** | 2008, 1917, 1897 | |
| **[Fe-Mn]** | 2019, 1930, 1912 | 1697 |
| **[Co-Mn]** | 2020, 1927, 1908 | 1642 |
| $Mn(bipy)(CO)_3Br$ | 2023, 1932, 1915 | |
| FeNO(bme-dach) | - | 1649 |
| CoNO(bme-dach) | - | 1594 |

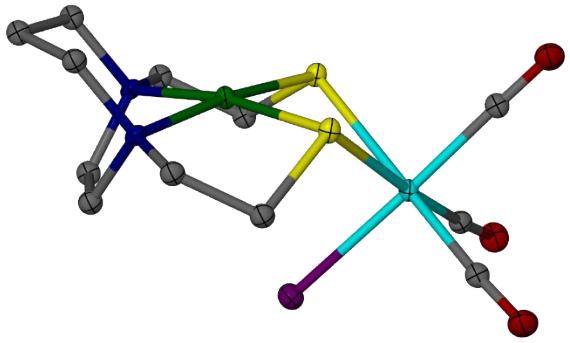

**Figure S37.** Thermal ellipsoid plots at 50% probability for **[Ni-Re]**.

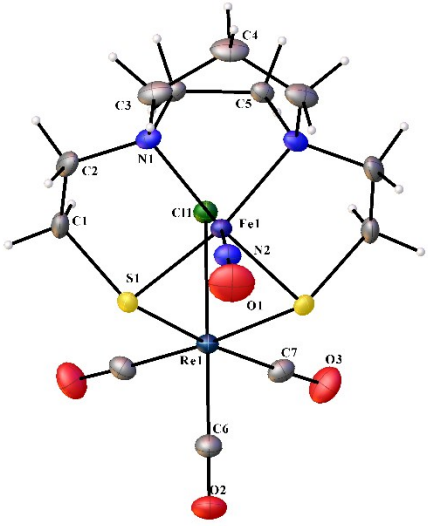


**Figure S38.** Thermal ellipsoid plots at 50% probability for **[Fe-Re]**.

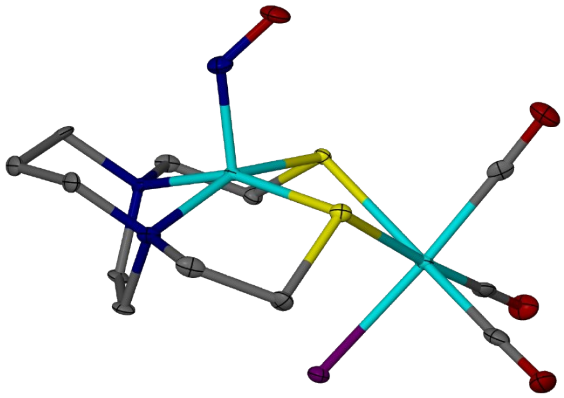

**Figure S39.** Thermal ellipsoid plots at 50% probability for **[Co-Re]**.

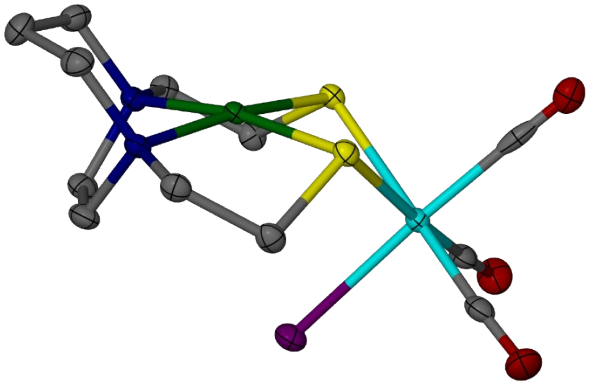

**Figure S40.** Thermal ellipsoid plots at 50% probability for **[Ni-Mn]**.

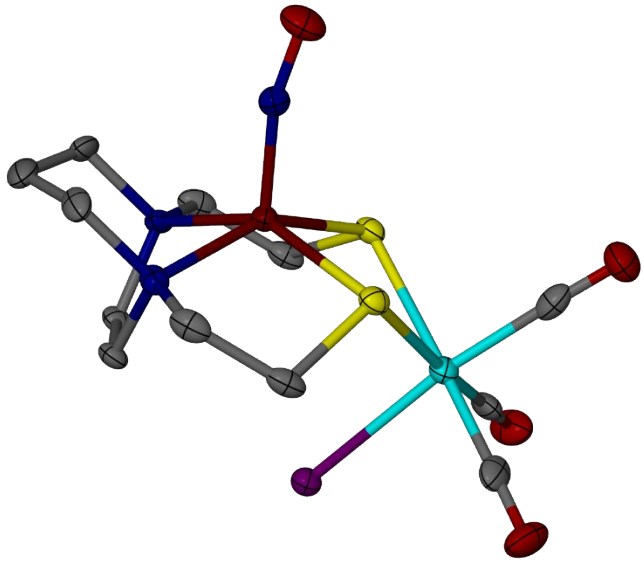

**Figure S41.** Thermal ellipsoid plots at 50% probability for **[Fe-Mn]**.

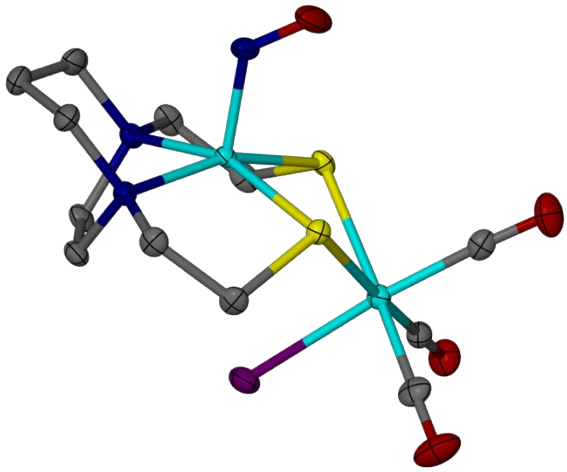

**Figure S42.** Thermal ellipsoid plots at 50% probability for **[Co-Mn]**.

**Table S4.** Crystal data and structure refinement for **[Ni-Re]**.

| | | |
|---|---|---|
| Identification code | nireb | |
| Empirical formula | C12 H18 Cl N2 Ni O3 Re S2 | |
| Formula weight | 582.76 | |
| Temperature | 110.15 K | |
| Wavelength | 1.54178 Å | |
| Crystal system | Orthorhombic | |
| Space group | Pnma | |
| Unit cell dimensions | a = 12.2999(4) Å | □= 90°. |
| | b = 12.3134(4) Å | □= 90°. |
| | c = 10.9388(6) Å | □ = 90°. |
| Volume | 1656.72(12) $Å^3$ | |
| Z | 4 | |
| Density (calculated) | 2.336 $Mg/m^3$ | |
| Absorption coefficient | 19.433 $mm^{-1}$ | |
| F(000) | 1120 | |
| Crystal size | 0.12 x 0.03 x 0.01 $mm^3$ | |
| Theta range for data collection | 5.409 to 60.754°. | |
| Index ranges | -13<=h<=13, -13<=k<=13, -12<=l<=12 | |
| Reflections collected | 32269 | |
| Independent reflections | 1328 [R(int) = 0.0769] | |
| Completeness to theta = 67.679° | 84.4 % | |
| Absorption correction | Semi-empirical from equivalents | |
| Max. and min. transmission | 0.4613 and 0.2122 | |
| Refinement method | Full-matrix least-squares on $F^2$ | |
| Data / restraints / parameters | 1328 / 37 / 110 | |
| Goodness-of-fit on $F^2$ | 1.102 | |
| Final R indices [I>2sigma(I)] | R1 = 0.0305, wR2 = 0.0740 | |
| R indices (all data) | R1 = 0.0318, wR2 = 0.0746 | |
| Extinction coefficient | n/a | |
| Largest diff. peak and hole | 1.203 and -1.280 $e.Å^{-3}$ | |

**Table S5.** Crystal data and structure refinement for **[Fe-Re]**.

| | | |
|---|---|---|
| Identification code | fenore | |
| Empirical formula | C12 H18 Cl Fe N3 O4 Re S2 | |
| Formula weight | 609.91 | |
| Temperature | 110.0 K | |
| Wavelength | 0.71073 Å | |
| Crystal system | Orthorhombic | |
| Space group | Pnma | |
| Unit cell dimensions | a = 18.8370(8) Å | □= 90°. |
| | b = 10.3101(4) Å | □= 90°. |
| | c = 9.3359(4) Å | □ = 90°. |
| Volume | 1813.14(13) $Å^3$ | |
| Z | 4 | |
| Density (calculated) | 2.234 $Mg/m^3$ | |
| Absorption coefficient | 7.869 $mm^{-1}$ | |
| F(000) | 1172 | |
| Crystal size | 0.25 x 0.25 x 0.1 $mm^3$ | |
| Theta range for data collection | 3.653 to 32.446°. | |
| Index ranges | -28<=h<=27, -15<=k<=15, -14<=l<=13 | |
| Reflections collected | 30754 | |
| Independent reflections | 3304 [R(int) = 0.0580] | |
| Completeness to theta = 26.000° | 99.6 % | |
| Absorption correction | Semi-empirical from equivalents | |
| Max. and min. transmission | 0.7464 and 0.3082 | |
| Refinement method | Full-matrix least-squares on $F^2$ | |
| Data / restraints / parameters | 3304 / 0 / 121 | |
| Goodness-of-fit on $F^2$ | 1.123 | |
| Final R indices [I>2sigma(I)] | R1 = 0.0240, wR2 = 0.0546 | |
| R indices (all data) | R1 = 0.0288, wR2 = 0.0563 | |
| Extinction coefficient | n/a | |
| Largest diff. peak and hole | 2.432 and -0.984 $e.Å^{-3}$ | |

**Table S6.** Crystal data and structure refinement for **[Co-Re]**.

| | | |
|---|---|---|
| Identification code | CodachRe | |
| Empirical formula | C16 H26 Cl Co N3 O5 Re S2 | |
| Formula weight | 685.10 | |
| Temperature | 110(2) K | |
| Wavelength | 1.54178 Å | |
| Crystal system | Monoclinic | |
| Space group | $P2_1/c$ | |
| Unit cell dimensions | a = 8.4344(4) Å | □= 90°. |
| | b = 22.0021(10) Å | □= 97.361(2)°. |
| | c = 11.9816(8) Å | □ = 90°. |
| Volume | 2205.2(2) $Å^3$ | |
| Z | 4 | |
| Density (calculated) | 2.064 $Mg/m^3$ | |
| Absorption coefficient | 19.640 $mm^{-1}$ | |
| F(000) | 1336 | |
| Crystal size | 0.575 x 0.025 x 0.025 $mm^3$ | |
| Theta range for data collection | 4.018 to 63.779°. | |
| Index ranges | -9<=h<=9, -25<=k<=25, -13<=l<=13 | |
| Reflections collected | 41925 | |
| Independent reflections | 3597 [R(int) = 0.0475] | |
| Completeness to theta = 63.779° | 99.3 % | |
| Absorption correction | Semi-empirical from equivalents | |
| Max. and min. transmission | 0.7524 and 0.3256 | |
| Refinement method | Full-matrix least-squares on $F^2$ | |
| Data / restraints / parameters | 3597 / 0 / 256 | |
| Goodness-of-fit on $F^2$ | 1.125 | |
| Final R indices [I>2sigma(I)] | R1 = 0.0255, wR2 = 0.0646 | |
| R indices (all data) | R1 = 0.0278, wR2 = 0.0698 | |
| Extinction coefficient | n/a | |
| Largest diff. peak and hole | 0.582 and -1.504 $e.Å^{-3}$ | |

**Table S7.** Crystal data and structure refinement for **[Ni-Mn]**.

| | | |
|---|---|---|
| Identification code | NidachMn | |
| Empirical formula | C12 H18 Br Mn N2 Ni O3 S2 | |
| Formula weight | 495.96 | |
| Temperature | 150(2) K | |
| Wavelength | 0.71073 Å | |
| Crystal system | Orthorhombic | |
| Space group | Pnma | |
| Unit cell dimensions | a = 12.4666(8) Å | □= 90°. |
| | b = 12.2823(7) Å | □= 90°. |
| | c = 10.8128(6) Å | □ = 90°. |
| Volume | 1655.64(17) $Å^3$ | |
| Z | 4 | |
| Density (calculated) | 1.990 $Mg/m^3$ | |
| Absorption coefficient | 4.576 $mm^{-1}$ | |
| F(000) | 992 | |
| Crystal size | 0.168 x 0.100 x 0.100 $mm^3$ | |
| Theta range for data collection | 2.493 to 27.520°. | |
| Index ranges | -16<=h<=16, -15<=k<=15, -14<=l<=14 | |
| Reflections collected | 24026 | |
| Independent reflections | 1994 [R(int) = 0.0780] | |
| Completeness to theta = 25.242° | 99.9 % | |
| Absorption correction | Semi-empirical from equivalents | |
| Max. and min. transmission | 0.6576 and 0.5136 | |
| Refinement method | Full-matrix least-squares on $F^2$ | |
| Data / restraints / parameters | 1994 / 3 / 119 | |
| Goodness-of-fit on $F^2$ | 1.085 | |
| Final R indices [I>2sigma(I)] | R1 = 0.0319, wR2 = 0.0763 | |
| R indices (all data) | R1 = 0.0432, wR2 = 0.0814 | |
| Extinction coefficient | n/a | |
| Largest diff. peak and hole | 0.553 and -0.687 $e.Å^{-3}$ | |

**Table S8.** Crystal data and structure refinement for **[Fe-Mn]**.

| | |
|---|---|
| Identification code | femnbr |
| Empirical formula | C12 H18 Br Fe Mn N3 O4 S2 |
| Formula weight | 523.11 |
| Temperature | 110.15 K |
| Wavelength | 1.54178 Å |
| Crystal system | Orthorhombic |
| Space group | Pnma |
| Unit cell dimensions | a = 18.6248(15) Å □= 90°. |
| | b = 10.8713(9) Å □= 90°. |
| | c = 9.1657(7) Å □ = 90°. |
| Volume | 1855.8(3) $Å^3$ |
| Z | 4 |
| Density (calculated) | 1.872 $Mg/m^3$ |
| Absorption coefficient | 16.632 $mm^{-1}$ |
| F(000) | 1044 |
| Crystal size | 0.08 x 0.07 x 0.01 $mm^3$ |
| Theta range for data collection | 4.748 to 60.719°. |
| Index ranges | -21<=h<=21, -12<=k<=12, -10<=l<=10 |
| Reflections collected | 22616 |
| Independent reflections | 1491 [R(int) = 0.0805] |
| Completeness to theta = 67.679° | 84.7 % |
| Absorption correction | Semi-empirical from equivalents |
| Max. and min. transmission | 0.7519 and 0.4851 |
| Refinement method | Full-matrix least-squares on $F^2$ |
| Data / restraints / parameters | 1491 / 0 / 121 |
| Goodness-of-fit on $F^2$ | 1.172 |
| Final R indices [I>2sigma(I)] | R1 = 0.0432, wR2 = 0.0897 |
| R indices (all data) | R1 = 0.0484, wR2 = 0.0917 |
| Extinction coefficient | n/a |
| Largest diff. peak and hole | 0.773 and -0.515 $e.Å^{-3}$ |

**Table S9.** Crystal data and structure refinement for **[Co-Mn]**.

| | | |
|---|---|---|
| Identification code | CodachMn | |
| Empirical formula | C24 H36 Br2 Co2 Mn2 N6 O8 S4 | |
| Formula weight | 1052.39 | |
| Temperature | 150(2) K | |
| Wavelength | 0.71073 Å | |
| Crystal system | Monoclinic | |
| Space group | $P2_1/n$ | |
| Unit cell dimensions | a = 7.5578(12) Å | □= 90°. |
| | b = 14.564(2) Å | □= 90.553(3)°. |
| | c = 32.747(5) Å | □ = 90°. |
| Volume | 3604.5(10) $Å^3$ | |
| Z | 4 | |
| Density (calculated) | 1.939 $Mg/m^3$ | |
| Absorption coefficient | 4.091 $mm^{-1}$ | |
| F(000) | 2096 | |
| Crystal size | 0.430 x 0.060 x 0.060 $mm^3$ | |
| Theta range for data collection | 1.530 to 27.567°. | |
| Index ranges | -9<=h<=9, -18<=k<=18, -42<=l<=42 | |
| Reflections collected | 90482 | |
| Independent reflections | 8308 [R(int) = 0.0565] | |
| Completeness to theta = 25.242° | 100.0 % | |
| Absorption correction | Semi-empirical from equivalents | |
| Max. and min. transmission | 0.7914 and 0.2722 | |
| Refinement method | Full-matrix least-squares on $F^2$ | |
| Data / restraints / parameters | 8308 / 0 / 433 | |
| Goodness-of-fit on $F^2$ | 1.087 | |
| Final R indices [I>2sigma(I)] | R1 = 0.0332, wR2 = 0.0825 | |
| R indices (all data) | R1 = 0.0416, wR2 = 0.0892 | |
| Extinction coefficient | n/a | |
| Largest diff. peak and hole | 0.826 and -1.077 $e.Å^{-3}$ | |

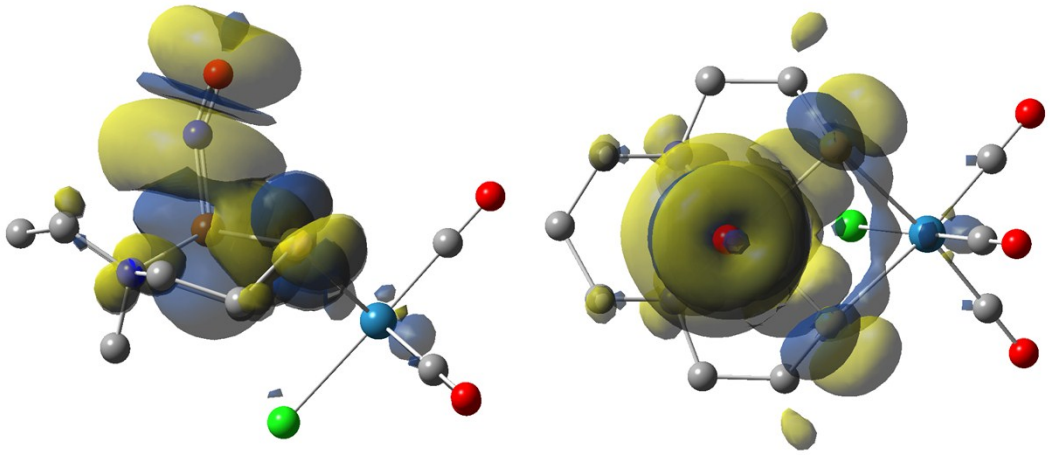

**Figure S43.** Spin density (isovalue: 0.0004) plot for [**Fe-Re**]. (Spin densities: Fe(NO): 0.911 (in which Fe: 1.907; NO: - 0.996 as they are antiferromagnetically coupled); Re: 0.035; other atoms: 0.054).

**Table S10.** The calculated CO stretching frequencies (unscaled).

| Species | $\upsilon_{CO}$ / $cm^{-1}$ | Species | $\upsilon_{CO}$ / $cm^{-1}$ | $\Delta\ \upsilon_{AVG}$ / $cm^{-1}$ |
|---|---|---|---|---|
| **[Fe-Re]** | 1981, 1992, 2084 | **[Fe-Re]$^-$** | 1943, 1946, 2054 | 38 |
| **[Co-Re]** | 1981, 1991, 2083 | **[Co-Re]$^-$** | 1944, 1947, 2054 | 37 |
| **[Ni-Re]** | 1976, 1988, 2082 | **[Ni-Re]$^-$** | 1935, 1939, 2047 | 42 |

## References


1. Chiang, C.-Y.; Lee, J.; Dalrymple, C.; Sarahan, M. C.; Reibenspies, J. H.; Darensbourg, M. Y., Synthesis and Molecular Structures of Mononitrosyl (N2S2)M(NO) Complexes (M = Fe, Co). *Inorg. Chem.* **2005,** *44* (24), 9007-9016.
2. Smee, J. J.; Miller, M. L.; Grapperhaus, C. A.; Reibenspies, J. H.; Darensbourg, M. Y., Subtle Bite-Angle Influences on N2S2Ni Complexes. *Inorg. Chem.* **2001,** *40* (14), 3601-3605.
3. Becke, A. D., Density-functional thermochemistry. III. The role of exact exchange. *J. Chem. Phys.* **1993,** *98* (7), 5648-5652.
4. Frisch, M. J.; Trucks, G. W.; Schlegel, H. B.; Scuseria, G. E.; Robb, M. A.; Cheeseman, J. R.; Scalmani, G.; Barone, V.; Mennucci, B.; Petersson, G. A.; Nakatsuji, H.; Caricato, M.; Li, X.; Hratchian, H. P.; Izmaylov, A. F.; Bloino, J.; Zheng, G.; Sonnenberg, J. L.; Hada, M.; Ehara, M.; Toyota, K.; Fukuda, R.; Hasegawa, J.; Ishida, M.; Nakajima, T.; Honda, Y.; Kitao, O.; Nakai, H.; Vreven, T.; Montgomery Jr., J. A.; Peralta, J. E.; Ogliaro, F.; Bearpark, M. J.; Heyd, J.; Brothers, E. N.; Kudin, K. N.; Staroverov, V. N.; Kobayashi, R.; Normand, J.; Raghavachari, K.; Rendell, A. P.; Burant, J. C.; Iyengar, S. S.; Tomasi, J.; Cossi, M.; Rega, N.; Millam, N. J.; Klene, M.; Knox, J. E.; Cross, J. B.; Bakken, V.; Adamo, C.; Jaramillo, J.; Gomperts, R.; Stratmann, R. E.; Yazyev, O.; Austin, A. J.; Cammi, R.; Pomelli, C.; Ochterski, J. W.; Martin, R. L.; Morokuma, K.; Zakrzewski, V. G.; Voth, G. A.; Salvador, P.; Dannenberg, J. J.; Dapprich, S.; Daniels, A. D.; Farkas, Ö.; Foresman, J. B.; Ortiz, J. V.; Cioslowski, J.; Fox, D. J. *Gaussian 09*, Gaussian, Inc.: Wallingford, CT, USA, 2009.

5. Krishnan, R.; Binkley, J. S.; Seeger, R.; Pople, J. A., Self-consistent molecular orbital methods. XX. A basis set for correlated wave functions. *J. Chem. Phys.* **1980,** *72* (1), 650-654.
6. McLean, A. D.; Chandler, G. S., Contracted Gaussian basis sets for molecular calculations. I. Second row atoms, Z=11–18. *J. Chem. Phys.* **1980,** *72* (10), 5639-5648.
7. Clark, T.; Chandrasekhar, J.; Spitznagel, G. W.; Schleyer, P. V. R., Efficient diffuse function-augmented basis sets for anion calculations. III. The 3-21+G basis set for first-row elements, Li–F. *J. Comput. Chem.* **1983,** *4* (3), 294-301.
8. Wachters, A. J. H., Gaussian Basis Set for Molecular Wavefunctions Containing Third-Row Atoms. *J. Chem. Phys.* **1970,** *52* (3), 1033-1036.
9. Hay, P. J., *J. Chem. Phys.* **1977,** *66*, 4377-4384.
10. Raghavachari, K.; Trucks, G. W., *J. Chem. Phys.* **1989,** *91*, 1062-1065.
11. Marenich, A. V.; Cramer, C. J.; Truhlar, D. G., Universal Solvation Model Based on Solute Electron Density and on a Continuum Model of the Solvent Defined by the Bulk Dielectric Constant and Atomic Surface Tensions. *The Journal of Physical Chemistry B* **2009,** *113* (18), 6378-6396.
12. APEX2, Bruker AXS Inc., Madison, WI, 2007.
13. SAINT, Bruker AXS Inc., Madison, WI, 2007.
14. Sheldrick, G., A short history of SHELX. *Acta Crystallographica Section A* **2008,** *64* (1), 112-122.
15. Barbour, L. J., *J. Supramol. Chem.* **2003,** *1*, 189-191.